CHAPTER 9

Impact of mutations in the SARS-CoV-2 spike RBD region of BA.1 and BA.2 variants on its interaction with ACE2 Receptor Protein

Impact of mutations in the SARS-CoV-2 spike RBD region of BA.1 and BA.2 variants on its interaction with ACE2 Receptor Protein

9.1. Abstract:

The COVID-19 pandemic started with the onset of 2020 and still thriving due to its continuous mutation and evolution into new strains. Omicron strain is been recently categorized as a variant of concern (VoC) by WHO and based on mutations it is divided into BA.1 and BA.2. In this study, we compared the interaction profile of RBD of spike protein of the BA.1 and BA.2 variant of SARS-CoV-2 with ACE2 receptor. From the molecular dynamic's simulation study, we observed the spike protein of BA.1 and BA.2 variant utilizes unique strategies to have a stable binding with ACE2. The binding affinity of spike protein of the BA.2 variant-ACE2 complex is indeed high (GB_{TOT}=-23.87 kcal/mol) in comparison with spike protein of BA.1 variant-ACE2 complex (GB_{TOT}=5.38 kcal/mol). Stable binding of spike protein to ACE2 is essential for virus entry and the interactions between them should be understood well for the treatment modalities.

9.2. Introduction:

In overdue December 2019, an endemic of a mysterious pneumonia characterized with fever, dry cough, and fatigue, and gastrointestinal issues came about in a seafood wholesale wet marketplace, the Huainan Seafood Wholesale Market, in Wuhan, Hubei, China [1]. Although the virus was hastily named 2019-nCoV, after which renamed SARS-CoV-2. Coronaviruses take their understand from the precise spikes with rounded pointers that enhance their surface, which reminded virologists of the appeal of the sun's atmosphere, noted as its corona [2]. The earliest recounted infected person fell sick on 1 December 2019. However, that person did not have a reference to the later wet marketplace cluster while within side the preceding case may moreover be handed off on 17 November. Two-thirds of the initial case cluster has been related with the marketplace [3]. Molecular clock evaluation indicates that the index case is perhaps too had been infected among mid-October and mid-November 2019. As of 6 May 2022, more than 6,272,189 deaths have been attributed to COVID-19 with the primary loss of life in Wuhan on 9th January 2020. These numbers range with the aid of community and over time, stimulated via way of means of sorting out volume, healthcare, treatment options, authorities' response, time for the cause that the initial outbreak, and population characteristics, including age, sex, and popular health [4,5].

ACE2 was identified as the access receptor for each SARS-CoV-2, and SARS-CoV. Structural research revealed that each SARS-CoV-2 and SARS-CoV spike (S) glycoproteins bind ACE2 with elevated affinity [6]. The shape of SARS-CoV-2 S-protein resembles that of SARS-CoV S-protein with the spike

RBD located contacting the extracellular vicinity of ACE2 which is surprisingly a big macromolecule with a diameter of 70 Å. SARS spike is its large mass (500 kD consistent with trimer) and striking, club-formed appearance, from the end-on, this seems like a 3-bladed propeller with a radius of 90 Å [7].

Genetic lineages of SARS-CoV-2 had been growing and circulating round the arena on the grounds of the COVID-19 pandemic. CoVs are enveloped viruses with fine sense ssRNA genomes with a cistern of approximately 26-32 kb, the largest genome length for an RNA virus. The SARS spike may be subdivided into 4 structural domain names (from N to C terminus); the 2 big outdoors domain names S1 and S2 are regularly chargeable for receptor binding and membrane fusion, respectively. The SARS spike appears to be insensitive to redox conditions [8]. For SARS-CoV, it is suggested that the virus is internalized within the cell by manner of endocytosis, and then exposed to a low pH environment. It is postulated that proteolytic cleavage among the S1 and S2 domain initiates the membrane fusion process [9-12]. The S protein of SARS-CoV-2 genome is of leading significance for ACE2 receptor binding and membrane fusion of the virus, and running medical research on healing techniques and at the formation of immune response [13-17]. Therefore, mutations that arise within the S protein, in specific the RBD within the S gene have ended in versions of corona virus. Some of the massive SARS-CoV-2 versions are Alpha (B.1.1.7, on the start placed within side the United Kingdom), Beta (B.1.351, first determined in South Africa), Epsilon (B.1.427 and B.1.429, first recognized in United States-California), Delta (B.1.617.2, first recognized in India), Gamma (P.1, first identified in Japan/Brazil).

Omicron was as quickly as first identified in Botswana and South Africa in a while scientist have been alerted to the World Health Organization (WHO) approximately the version on November 24, 2021. On 26 November 2021, WHO declared the strain as “Variant of Concern (VOC)” because of its excessive ease of transmission [18]. The genomic series evaluation has showed over 30 mutations in Omicron in difference to the unique SARS-CoV-2 strain. BA.1 is the maximum prolific sub lineage, detected in maximum international regions worldwide and presently accounting for 99% of instances in the United States. BA.2 is much less prolific, as a substitute has overtaken BA.1 in Denmark, Nepal, and the Philippines as the maximum detected version, and has a minor presence in India, the United Kingdom, and infinite specific countries. The third sub-lineage BA.3 is but to take off globally, absolutely accounting for numerous hundred conditions on the most [19]. Triad, a grow to be aware about that denotes 3 mutations, the D614G mutation within the Spike protein, the P323L mutation in NSP12 polymerase, and the C241U noncoding mutation within 5’ end. The Triad is the founding version of all variations of venture viruses. Omicron (BA.1) is already identified to have a few extraordinary innate sojourns relative to the mutated strains [20]. Most strikingly, 2.7-3.7-fold is more transmissible than Delta. Moreover, the affinity of the BA.1 Spike for the ACE2 receptor is absolutely two times as

excessive because the Wuhan strain [21]. The first cluster consists of receptor-binding mutations G339D, S371F/L, S373P, and S375F. The second cluster consists of receptor-binding region mutations Q493R, G496S, Q498R, and Y505H. The 1/3 consists of fusion region mutations N764K, N856K, Q954H, N969K, and L981F. The aggregate of these clusters results in high binding affinity of the S-protein and ACE2 and hence gain access to enter in the cell. Out of the 3 mutations, G496S, N856K, and L981F, are determined completely in BA.1, not BA.2 or BA.3 [16]. Henceforth, we aspire to seem into comparative structural evaluation of the two sub-versions of omicron BA.1 and BA.2 binding affinities with ACE2 deploying MD simulation and computational programs.

9.3. Materials and Methods:

The 3-D structure of the SARS-CoV-2 receptor-binding domain of BA.1 (**Figure 9.1A**) and BA.2 (**Figure 9.1B**) variants bound with ACE2 were obtained by inducing punctual mutation in the 3-D structure of SARS-CoV-2 spike receptor-binding domain bound with ACE2 (S protein-ACE2) (PDB ID: 6LZG with a resolution of 2.50 Å retrieved from the Research Collaboratory for Structural Bioinformatics Protein Data bank (www.rcsb.org) [22] using UCSF Chimera package alpha v.1.12 [23].The punctual mutations induced in the 6LZG to construct the BA.1 and BA.2 are shown in **Table 9.1**. Both the complex structures were then energy minimized using steepest descents followed by conjugate gradient minimization technique.

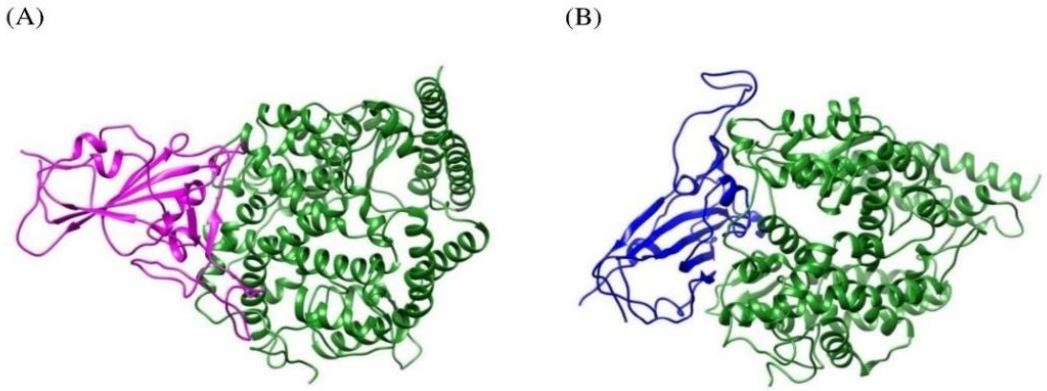

Figure 9.1. *3D structure of* ***(A)*** *SARS-CoV-2 spike receptor-binding domain of BA.1 variant bound with ACE2 (S protein (BA.1)-ACE2)* ***(B)*** *SARS-CoV-2 spike receptor-binding domain of BA.2 variant bound with ACE2 (S protein (BA.2)-ACE2).*

Table 9.1. *Showing mutations (in RBD of Spike Protein) of BA.1 and BA.2 lineages*

Mutations of BA.1 lineages	Mutations of BA.2 lineages	Common mutations of BA.1 and BA.2 lineages
G339D, S373P, K417N, N440K, S477N, T478K, E484A, Q493R, Q498R, N501Y, Y505H, **S371L, G446S, G496S**, S375F.	G339D, S373P, K417N, N440K, S477N, T478K, E484A, Q493R, Q498R, N501Y, Y505H, S375F, **S371F, T376A, D405N, R408S.**	G339D, S373P, K417N, N440K, S477N, T478K, E484A, Q493R, Q498R, N501Y, Y505H, S375F.

9.3.1.Molecular Dynamics Simulations.

The BA.1 type as well as the BA.2 of the complex of SARS-CoV-2 spike receptor-binding domain bound with ACE2 were subjected to MD simulations. The MD simulation was performed using AMBER ff14SB force field with AMBER software package [24]. To ensure the overall neutrality of the two complex systems, appropriate numbers of counter ions were added. The two complex systems were subjected to MD simulations in explicit solvent, and were solvated with TIP3P [25] water model with a solvent buffer of 10 Å in all directions. In the first step of minimization, spike receptor-binding domain and ACE2 were fixed with a 500 kcal/mol/Å^2, and minimized the energy of all water molecules and counterions for 10000 steps of steepest descents (SD) followed by 10000 steps of the conjugate gradient (CG). Subsequently in the second step of minimization, to remove conflicting contacts the entire complex systems was repeated for 12000 steps of SD minimization and 8000 steps of CG minimization. Next, both the complex systems were gradually heated from 0-300 K in constant volume (NVT) conditions, thereby applying harmonic restraints with a force constant of 10 kcal/mol/Å^2 on the solute atoms, and equilibration was performed three times with 3000 ps using a force constant of 5.0 kcal/mol/Å . Finally, 50 ns MD simulations were performed using the NPT ensemble without restraints. We used the Particle mesh Ewald [26,27] technique with a non-bonded cutoff of 12.0 Å to limit the direct space sum to treat the long-range electrostatic interactions. All the bonds present in the system were constrained using the SHAKE algorithm [28]. The pressure and temperature (0.5 ps of heat bath and 0.2 ps of pressure relaxation) were kept constant by the Berendsen weak coupling algorithm [29] throughout the simulation process. The time step of MD simulation was set to 2 fs, and sampling was performed every 10 ps into the MD file.

After completion of the 50 ns of production dynamics of the complexes, the lowest energy conformer of the individual complex (S protein (BA.1)-ACE2 and S protein (BA.2)-ACE2) was extracted out using

the RMSD clustering algorithm from the highly populated clusters and submitted to PDBsum server (http://www.ebi.ac.uk/thornton srv/ databases /pdbsum/ Generate. html) to analyse for their residue-specific interactions which are considered to be important to know about the nature of interactions. PDBsum [30] is a database that, among other things, shows schematic diagrams of the non-bonded contacts between amino acid residues at the interface of molecules in a multimer complex.Snapshots of SARS-CoV-2 ACE2-Spike Protein (BA.1 and BA.2 variant) structures at discrete distance of separation (in Å) between their centre of mass are shown in **Figure 9.2 and 9.3.**

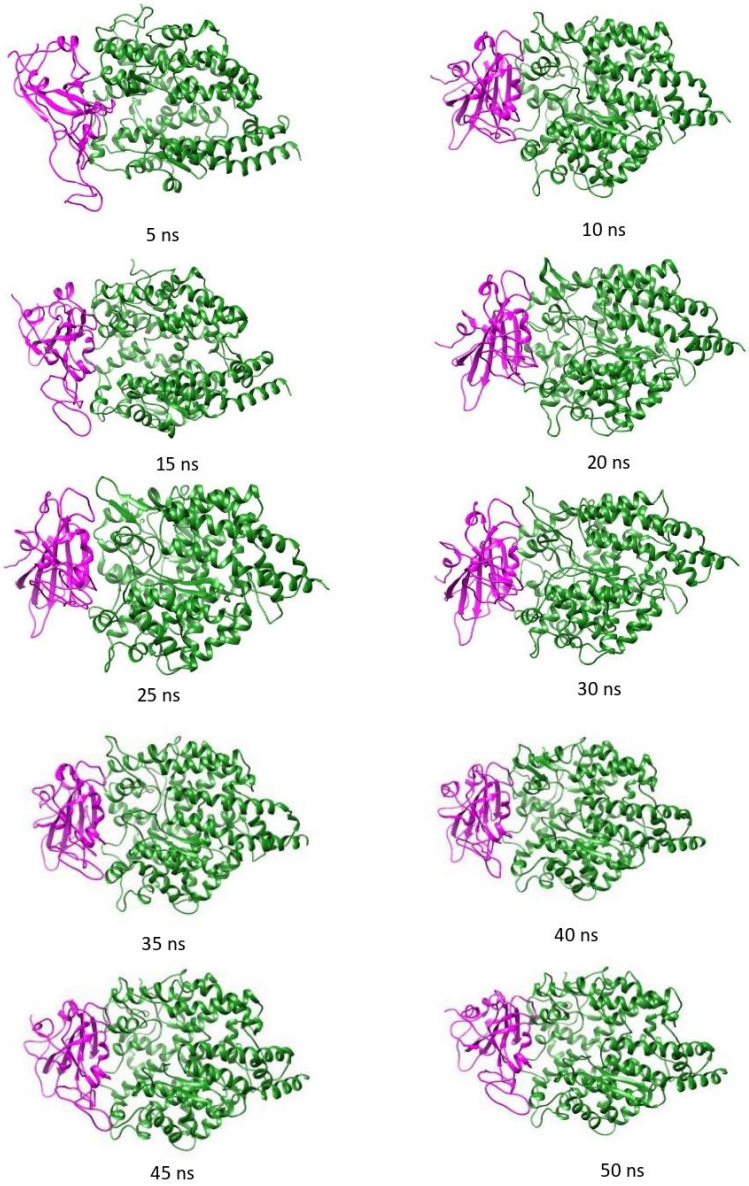

Figure 9.2. *Snapshots of SARS-CoV-2 ACE2-Spike Protein (BA.1 variant) structures at discrete distance of separation (in Å) between their centre of mass.*

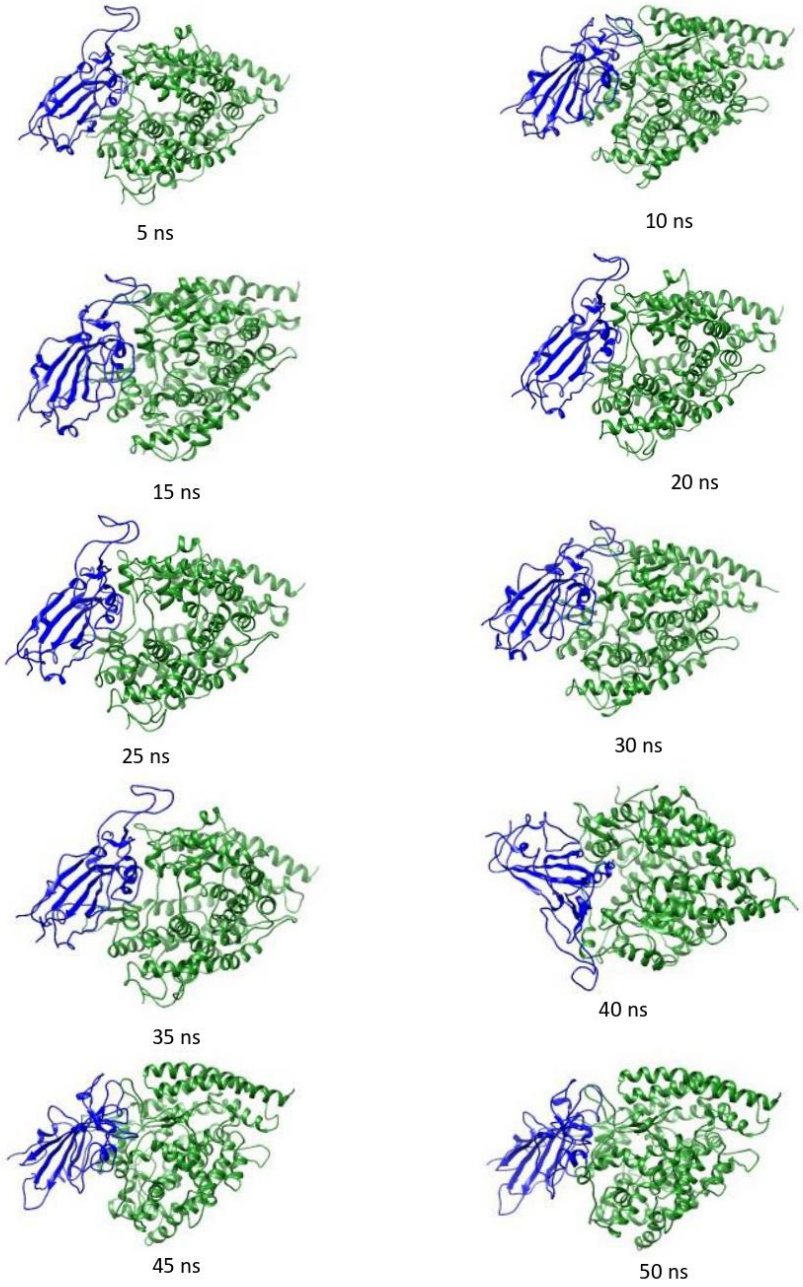

Figure 9.3. *Snapshots of SARS-CoV-2 ACE2-Spike Protein (BA.2 variant) structures at discrete distance of separation (in Å) between their centre of mass.*

9.3.2.Binding Free energy calculations.

The Molecular Mechanics Generalized Born Surface Area (MM-GBSA) method implemented in AMBER 16 [31,32] package was performed to calculate the binding free energy as well as the free energy decomposition of the two complex systems (S protein(BA.1)-ACE2 and S protein(BA.2)-

ACE2). For each complex system, 200 snapshots were selected from the last 10 ns of MD trajectories to calculate the relevant energies.

The formulas for calculating the BFE and their decomposed energetic components are same as shown in section 7A.3.2. of Chapter 7A [33,34]. The approaches and protocols that we have considered in this study to estimate the binding free energy have been used in many of the recent in-silico studies. [35-44].

9.4. Results and Discussion

9.4.1. MD simulation of the BA.1 and B.A.2 structure of SARS-CoV-2 spike receptor-binding domain bound with ACE2.

To study the dynamic properties of the two complexes BA.1and B.A.2 of SARS-CoV-2 spike receptor-binding domain bound with ACE2 we carried out 50 ns of MD simulation.

9.4.1.1. RMSD Analysis.

To test the stability of the (S protein (BA.1)-ACE2) and (S protein (BA.2)-ACE2) complexes, 50 ns of MD simulation studies were carried out. The conformational snapshots of the (S protein (BA.1)-ACE2) and (S protein (BA.2)-ACE2) complexes during the course of 50 ns MD simulation time were depicted in **Figure 9.2 and 9.3**. The average deviations in the atomic positions and the stability through the trajectory of 50 ns of the MD simulations, the RMSD (root mean square deviation) values of the backbone atoms of the complexes along with the S protein (Apo form) for both BA.1 and BA.2 were calculated (**Figure 9.4 and 9.5**). The RMSD of BA.1 type as well as the BA.2 complex appeared to be stable after 10 ns, revealing that good convergence was achieved for each system. Interestingly, we noticed that the RMSD values of the BA.2 complex were slightly smaller than that of the BA.1type complex. The average RMSD value of S protein (BA.1)-ACE2 and S protein (BA.2)-ACE2 type complex structure were calculated to be 1.41 Å (± 0.62) and 1.07 Å (± 0.62) respectively, which could indicate greater stability of the BA.2 complex structure. We observed significant differences in the conformational dynamics of S protein (BA.1/BA.2)-ACE2 complexes in the region in and around the mutation sites as shown in **Figures 9.6, 9.7 & 9.8**. We also noticed that the binding of ACE2 reduced the perturbation of S protein to a significant extent in both the complex systems.

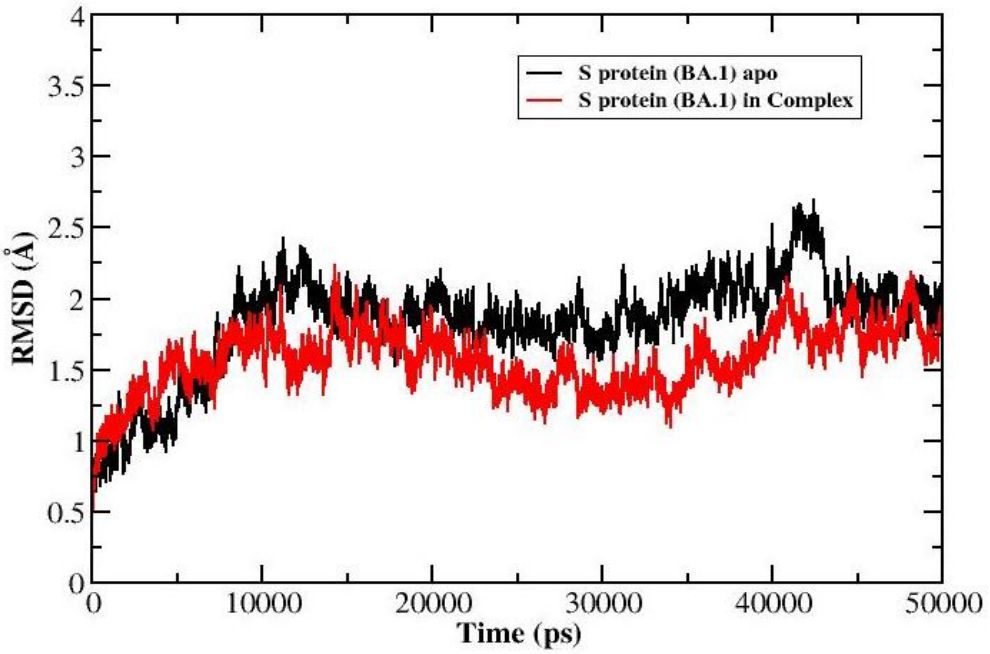

Figure 9.4. *Backbone RMSD's for S protein (BA.1) Apo (black) and S protein (BA.1)-ACE2 complex (red)*

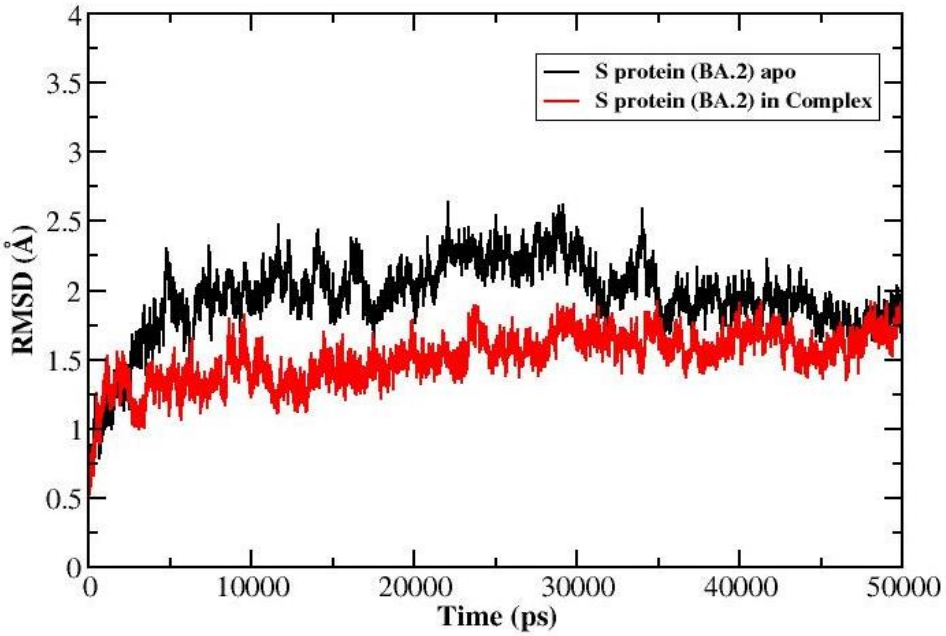

Figure 9. 5*. Backbone RMSD's for S protein (BA.2) Apo (black) and S protein (BA.2)-ACE2 complex (red)*

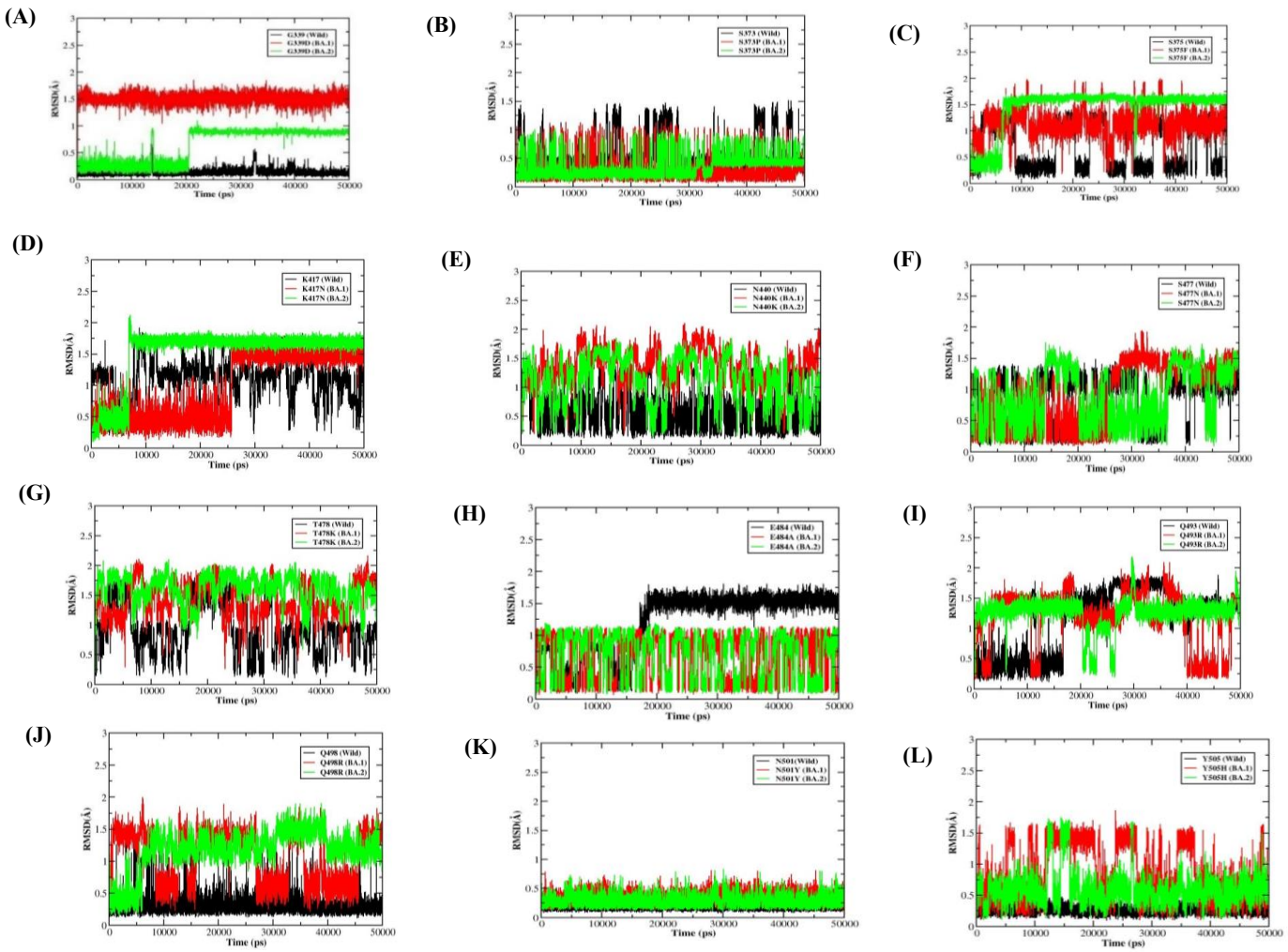

Figure 9.6. *RMSD plot of the common mutated residues at position* ***(A)*** *339* ***(B)*** *373* ***(C)*** *375* ***(D)*** *417* ***(E)*** *440* ***(F)*** *477* ***(G)****478* ***(H)****484* ***(I)****493* ***(J)****498* ***(K)****501* ***(L)*** *505 in S protein (WILD)-ACE2 complex (black), S protein (BA.1)-ACE2 complex (red) and S protein (BA.2)-ACE2 complex (green)*

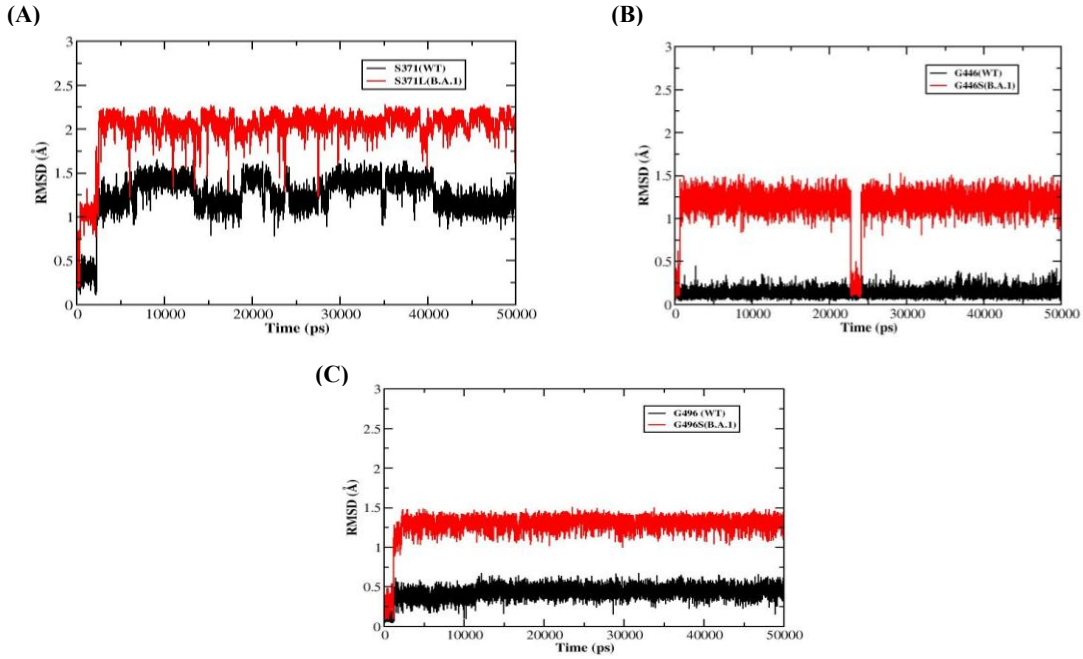

Figure 9.7. *RMSD plot of the residues exclusively present in BA.1at position* ***(A)*** *371* ***(B)*** *446* ***(C)*** *496 in S protein (WILD)-ACE2 complex (black), S protein (BA.1)-ACE2 complex (red).*

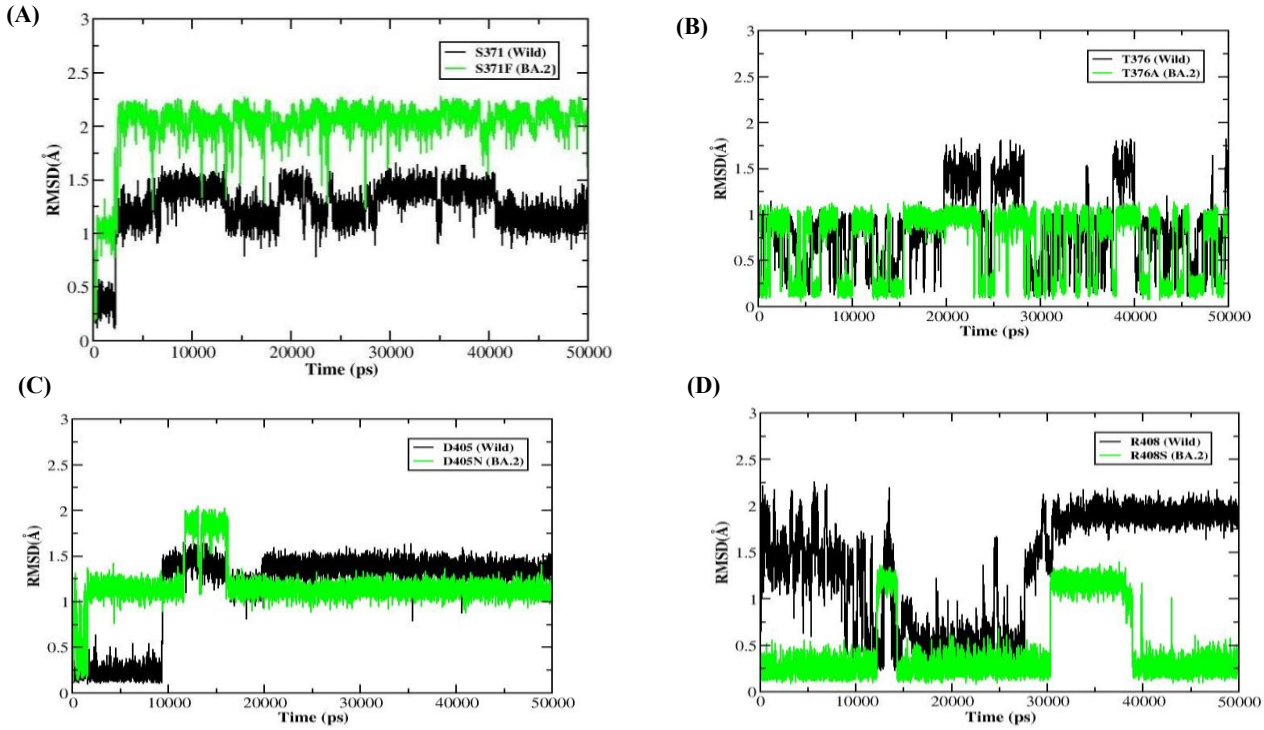

Figure 9.8. *RMSD plot of the residues exclusively present in BA.2 at position* ***(A)*** *371* ***(B)*** *376* ***(C)*** *405* ***(D)*** *408 in S protein (WILD)-ACE2 complex (black), S protein (BA.2)-ACE2 complex (green).*

9.4.1.2. RMSF Analysis

We further explored the S protein flexibility by RMSF values of the Cα from the MD simulations of the (S protein (BA.1)-ACE2) and (S protein (BA.2)-ACE2) complexes along with the wild type complex shown in **Figure 9.9**. We observed significant differences in the flexibility of S protein in BA.1, BA.2 and wild type complexes in particular at the regions in and around the mutation sites mentioned in the Table 9.1. The RMSF values of Cα atoms of S protein in BA.1 and BA.2 complexes shows relatively lower values than in the wild type complex [44]. From **Figure 9.9**, it is more apparent that there is significant reduction in structural fluctuations and increased stability in the case of BA.1 and BA.2 complexes. Among BA.1 and BA.2 complexes we found the fluctuations are relatively less in the case of BA.2 complex.

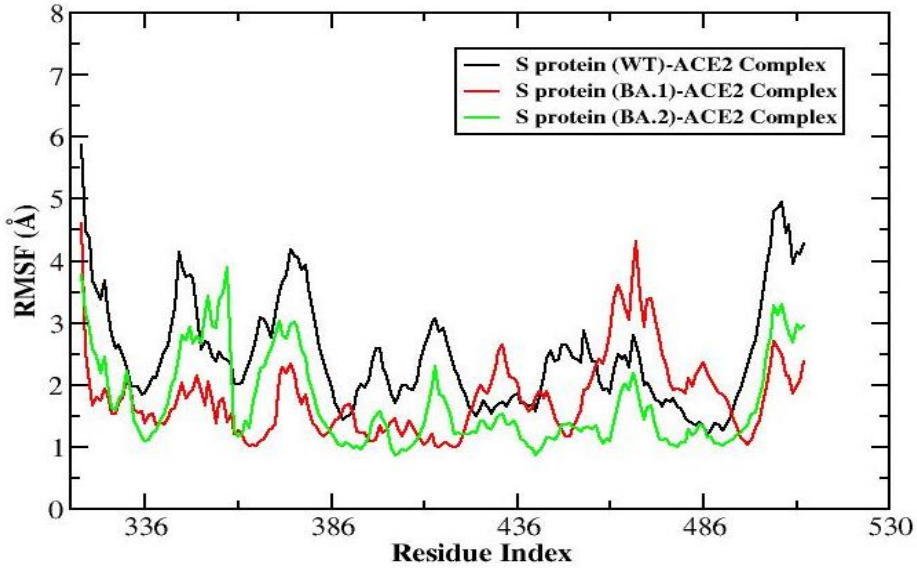

Figure 9.9. *Backbone RMSF's for S protein in* ***(A)*** *S protein (WILD)-ACE2 complex (black)* ***(B)*** *S protein (BA.1)-ACE2 complex (red) and* ***(C)*** *S protein (BA.2)-ACE2 complex (green).*

9.4.1.3. Hydrogen bond Analysis

Additionally, we also calculated and plotted the number of intermolecular hydrogen bonds present in the (S protein (BA.1)-ACE2) and (S protein (BA.2)-ACE2) complexes (**Figure 9.10**), as these hydrogen bonds play a crucial role in conferring the stability to the protein complexes. The number of inter-molecular hydrogen bonds was found to be higher in S protein (BA.2)-ACE2 complex than in S protein (BA.1)-ACE2 complex.

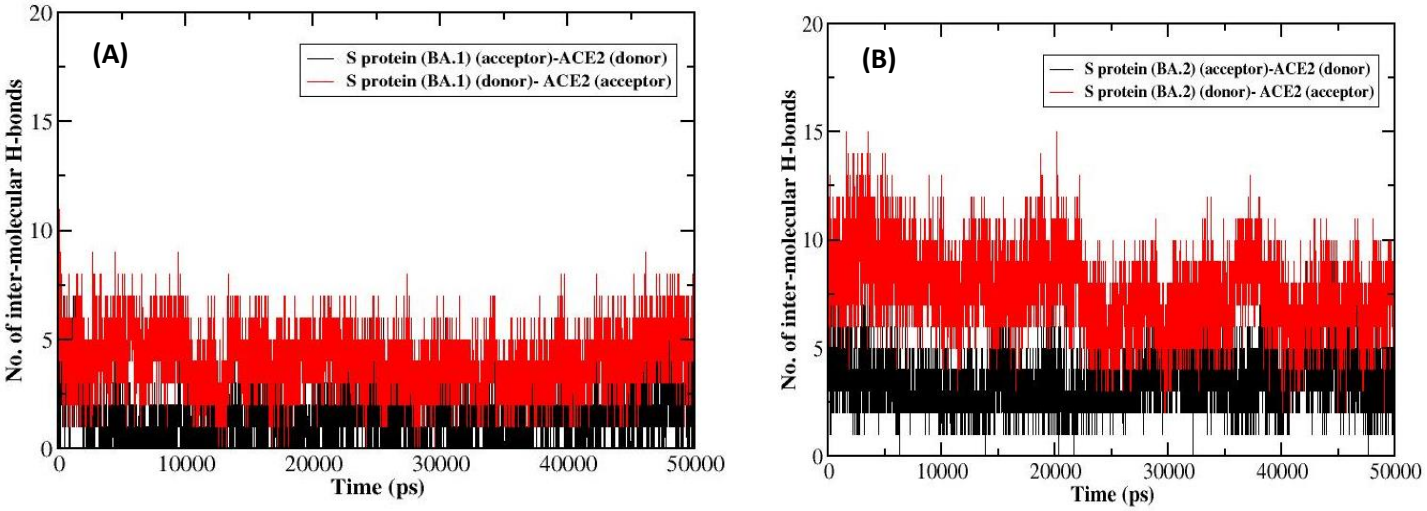

Figure 9.10. *Number of intermolecular hydrogen bonds between S protein and ACE2 in* ***(A)*** *S protein (BA.1)-ACE2 complex* ***(B)*** *S protein (BA.2)-ACE2 complex.*

The list of intermolecular hydrogen bonds noticed between the S protein (acceptor/donor) and ACE2 (donor/acceptor) during the last 20 ns of MD simulation of both the complexes were summarized in **Table 9.2- 9.5.**

Table 9.2. *Hydrogen bond analysis of S protein (BA.1)-ACE2 complex during the last 20 ns of MD simulation with S protein as acceptor and ACE2 as donor.*

Acceptor	DonorH	Donor	Frac	Average Distance (Å)	Average Angles (°)
GLY_49@O	GLN_464@HE22	GLN_464@NE2	0.2397	2.864	160.9005
TYR_169@O	GLN_316@HE22	GLN_316@NE2	0.2082	2.8367	159.4083
THR_168@O	GLN_316@HE21	GLN_316@NE2	0.157	2.8488	158.5888
ASP_95@OD2	ASN_467@H	ASN_467@N	0.1356	2.8779	162.9477
PRO_167@O	GLN_316@HE21	GLN_316@NE2	0.1101	2.8452	150.8264
PHE_43@O	LEU_333@H	LEU_333@N	0.0498	2.8725	158.9543
ASP_95@OD1	ASN_467@H	ASN_467@N	0.0443	2.8669	163.789
THR_168@O	GLN_316@HE22	GLN_316@NE2	0.0406	2.8536	159.5178
SER_51@OG	ASN_427@HD21	ASN_427@ND2	0.0329	2.8969	159.1247
THR_98@OG1	GLN_464@HE22	GLN_464@NE2	0.0284	2.8917	161.8117
VAL_171@H	GLU_317@HG2	GLU_317@CG	0.0256	2.8624	148.8493
PRO_167@O	ASN_314@HD21	ASN_314@ND2	0.0247	2.85	157.4171
GLY_170@HA2	GLN_316@HB3	GLN_316@CB	0.0184	2.9379	144.3039
ARG_76@HB3	ASN_331@HD21	ASN_331@ND2	0.014	2.8186	152.93
LYS_46@HE3	ASN_331@HA	ASN_331@CA	0.0136	2.8803	141.7735
VAL_75@HG13	ASN_331@HD21	ASN_331@ND2	0.0132	2.8503	149.1277
ASP_95@O	ASN_467@H	ASN_467@N	0.013	2.8928	159.6823
THR_53@HG1	ALA_428@HA	ALA_428@CA	0.0117	2.8968	144.0213
ASP_96@HB3	PRO_466@HD3	PRO_466@CD	0.0112	2.9266	140.7922
VAL_75@HG12	ASN_331@HD21	ASN_331@ND2	0.0098	2.8589	149.7488

GLN_174@HE22	GLN_316@HE22	GLN_316@NE2	0.0082	2.8593	142.0411
ASN_38@OD1	TYR_432@HH	TYR_432@OH	0.0081	2.7748	161.4923
CYX_47@O	SER_457@HG	SER_457@OG	0.0081	2.7697	159.6387
PRO_80@O	ASN_467@HD22	ASN_467@ND2	0.0077	2.8665	163.6005
LEU_58@HD23	GLN_464@HE21	GLN_464@NE2	0.0074	2.8469	153.3379
THR_44@HB	ASN_331@HB3	ASN_331@CB	0.0071	2.9447	144.2455
VAL_75@HG11	ASN_331@HD21	ASN_331@ND2	0.0065	2.842	149.4356
PHE_45@HB3	LEU_333@HB2	LEU_333@CB	0.0061	2.9458	142.1613
PHE_45@H	LEU_333@HD11	LEU_333@CD1	0.005	2.8183	150.3143
GLY_49@HA2	GLY_463@HA3	GLY_463@CA	0.0049	2.932	141.9332
LEU_58@HD22	GLN_464@HE21	GLN_464@NE2	0.0048	2.8426	152.5831
ASP_96@HB3	PRO_466@HB3	PRO_466@CB	0.0043	2.9506	138.558
LEU_58@HD21	GLN_464@HE21	GLN_464@NE2	0.0041	2.8282	153.2695
GLY_170@HA3	GLN_316@HB3	GLN_316@CB	0.0039	2.9488	144.0922
VAL_171@HG13	ASN_314@HD21	ASN_314@ND2	0.0038	2.8107	147.9498
PHE_45@H	LEU_333@HD13	LEU_333@CD1	0.0035	2.8086	150.7565
SER_51@HB3	ASN_427@HD21	ASN_427@ND2	0.0034	2.8505	143.4813
PHE_43@O	SER_332@HG	SER_332@OG	0.003	2.7707	161.5707
TYR_48@HD2	SER_457@HB3	SER_457@CB	0.003	2.9499	141.5948
GLY_49@HA3	GLN_464@HG2	GLN_464@CG	0.003	2.9444	142.1123
PHE_42@HE1	LEU_333@HG	LEU_333@CG	0.0026	2.9521	141.9051
SER_51@HB2	ASN_427@HD21	ASN_427@ND2	0.0026	2.8404	144.7371
SER_51@HG	ASN_427@HD21	ASN_427@ND2	0.0026	2.9053	144.1853
THR_98@OG1	GLN_464@HE21	GLN_464@NE2	0.0024	2.8839	156.8871
ASN_128@HD22	VAL_475@HG11	VAL_475@CG1	0.0024	2.9064	144.2958
LYS_46@HD2	ASN_331@HA	ASN_331@CA	0.002	2.9619	142.7854
THR_83@HG1	THR_542@HB	THR_542@CB	0.002	2.9449	147.5527
LEU_58@HD11	GLN_464@HE21	GLN_464@NE2	0.0019	2.8837	147.7311
TYR_48@HD2	SER_457@HB2	SER_457@CB	0.0018	2.9331	142.9105
THR_53@O	ASN_427@HD21	ASN_427@ND2	0.0017	2.892	157.6533
ASP_95@HB3	PRO_466@HB3	PRO_466@CB	0.0017	2.9475	139.9677
TYR_48@HE2	SER_457@HB2	SER_457@CB	0.0016	2.9313	140.3828
ASN_128@HD22	VAL_475@HG23	VAL_475@CG2	0.0016	2.9297	147.5273
PHE_42@HE1	LEU_333@HB3	LEU_333@CB	0.0015	2.9321	139.8203
PHE_45@H	LEU_333@HD23	LEU_333@CD2	0.0015	2.8588	144.6686
ASN_128@HD21	VAL_475@HG13	VAL_475@CG1	0.0015	2.8928	144.301
THR_44@HG22	ASN_331@HB3	ASN_331@CB	0.0014	2.9481	141.456
PHE_45@H	LEU_333@HD12	LEU_333@CD1	0.0014	2.7833	144.1054
TYR_48@HE2	SER_457@HB3	SER_457@CB	0.0014	2.9376	139.0274
ASP_95@HB3	ASN_467@H	ASN_467@N	0.0014	2.864	146.77
ASP_96@HB3	PRO_466@HG3	PRO_466@CG	0.0014	2.9378	140.7272
ASN_128@HD21	VAL_475@HG11	VAL_475@CG1	0.0014	2.8328	143.0306
ARG_76@HA	ASN_331@HD21	ASN_331@ND2	0.0013	2.8863	148.436
LEU_185@HD21	GLN_464@HE21	GLN_464@NE2	0.0013	2.8357	147.5448
THR_44@HA	SER_332@HA	SER_332@CA	0.0012	2.9504	149.0557

LYS_46@HE2	ASN_331@HA	ASN_331@CA	0.0012	2.9238	143.2173
ASN_128@HD22	VAL_475@HG12	VAL_475@CG1	0.0012	2.9159	141.1953
THR_44@HG1	ASN_331@HB3	ASN_331@CB	0.0011	2.8829	151.2197
PHE_45@HB3	LEU_333@HG	LEU_333@CG	0.0011	2.9703	141.2827
SER_51@HG	ALA_428@HA	ALA_428@CA	0.0011	2.8708	140.5887
THR_98@HG22	GLN_464@HE22	GLN_464@NE2	0.0011	2.8964	141.2293
THR_98@HG23	GLN_464@HG2	GLN_464@CG	0.0011	2.9577	142.4567
VAL_171@H	LEU_319@HG	LEU_319@CG	0.0011	2.8597	150.0912
VAL_171@HG22	GLU_317@HA	GLU_317@CA	0.0011	2.929	145.6942
TYR_37@HH	LEU_333@HD22	LEU_333@CD2	0.001	2.9222	144.0308
PHE_42@HE1	LEU_333@HD13	LEU_333@CD1	0.001	2.945	139.593
VAL_75@HG22	ASN_331@HD21	ASN_331@ND2	0.001	2.7666	142.7799
VAL_171@HG11	GLU_317@HG3	GLU_317@CG	0.001	2.9361	141.8414
VAL_171@HG13	GLU_317@HG2	GLU_317@CG	0.001	2.9564	140.5828
VAL_171@HG23	GLU_317@HA	GLU_317@CA	0.001	2.9521	147.3366
LEU_185@HD23	GLN_464@HE21	GLN_464@NE2	0.001	2.8325	145.2162

Table 9.3. *Hydrogen bond analysis of S protein (BA.1)-ACE2 complex during the last 20 ns of MD simulation with S protein as donor and ACE2 as acceptor.*

Acceptor	DonorH	Donor	Frac	Average Distance (Å)	Average Angles (°)
GLU_327@OE1	ARG_76@HH11	ARG_76@NH1	0.7025	2.7958	161.2338
GLU_327@OE2	ARG_76@HE	ARG_76@NE	0.6838	2.8227	161.2765
ASN_331@O	PHE_45@H	PHE_45@N	0.5423	2.8656	158.1682
ASN_427@O	THR_53@HG1	THR_53@OG1	0.4837	2.7391	161.9292
ASN_427@OD1	SER_51@HG	SER_51@OG	0.2479	2.7516	160.3904
ASN_331@O	THR_44@HG1	THR_44@OG1	0.1381	2.7299	162.964
GLN_316@O	VAL_171@H	VAL_171@N	0.1161	2.9052	160.6858
GLU_327@OE2	ARG_76@HH11	ARG_76@NH1	0.0875	2.8355	150.6311
GLU_317@OE1	GLN_174@HE21	GLN_174@NE2	0.0833	2.8346	160.3588
ASN_427@O	SER_51@HG	SER_51@OG	0.0813	2.7699	158.3964
GLU_317@OE2	GLN_174@HE21	GLN_174@NE2	0.0613	2.8321	160.413
ASN_331@OD1	LYS_46@HZ1	LYS_46@NZ	0.0566	2.8251	153.3407
GLU_327@OE1	ARG_76@HE	ARG_76@NE	0.0546	2.8737	150.8037
ASN_331@OD1	LYS_46@HZ2	LYS_46@NZ	0.0439	2.8292	152.0606
ASN_331@OD1	LYS_46@HZ3	LYS_46@NZ	0.0423	2.8211	153.1969
GLU_317@HG2	VAL_171@H	VAL_171@N	0.0373	2.854	156.5184
ASN_331@HA	LYS_46@HE3	LYS_46@CE	0.0325	2.8989	147.7269
ALA_428@O	THR_53@HG1	THR_53@OG1	0.03	2.7931	158.4839
GLU_327@OE2	ARG_76@HH21	ARG_76@NH2	0.0269	2.8163	157.2369
ALA_330@O	LYS_46@HZ2	LYS_46@NZ	0.0215	2.8361	152.8299
ALA_330@O	LYS_46@HZ1	LYS_46@NZ	0.0215	2.8409	153.4074
ASN_427@OD1	THR_53@HG1	THR_53@OG1	0.0193	2.7568	157.1427
ALA_330@O	LYS_46@HZ3	LYS_46@NZ	0.0192	2.8427	151.0891
PRO_466@HD3	ASP_96@HB3	ASP_96@CB	0.0154	2.9328	140.5884

GLN_316@HB3	GLY_170@HA2	GLY_170@CA	0.0135	2.9417	146.5182
GLN_316@HE22	GLN_174@HE22	GLN_174@NE2	0.0135	2.8863	141.7449
LEU_333@HD11	PHE_45@H	PHE_45@N	0.0115	2.8022	151.1491
LEU_333@HD13	PHE_45@H	PHE_45@N	0.0106	2.7901	150.7829
ASN_331@HD21	ARG_76@HB3	ARG_76@CB	0.0091	2.8072	147.075
ASP_472@OD1	LYS_130@HZ2	LYS_130@NZ	0.0091	2.8227	158.888
SER_457@OG	LYS_46@HZ1	LYS_46@NZ	0.009	2.895	157.0052
LEU_333@HD12	PHE_45@H	PHE_45@N	0.0083	2.8029	151.9859
GLY_463@HA3	GLY_49@HA2	GLY_49@CA	0.0082	2.9389	146.3336
LEU_333@HD21	PHE_45@H	PHE_45@N	0.008	2.8444	155.0599
ASN_331@HB3	THR_44@HB	THR_44@CB	0.0075	2.9383	139.8947
GLN_316@OE1	GLY_170@H	GLY_170@N	0.0072	2.8642	152.2153
ASN_427@OD1	LYS_54@HZ2	LYS_54@NZ	0.0072	2.8145	155.5906
GLU_327@OE1	ARG_76@HH21	ARG_76@NH2	0.0071	2.7995	152.8337
GLN_316@OE1	GLN_174@HE21	GLN_174@NE2	0.0066	2.8425	149.1729
SER_457@OG	LYS_46@HZ2	LYS_46@NZ	0.0063	2.8702	149.8814
LEU_333@HD22	PHE_45@H	PHE_45@N	0.0059	2.8145	154.1179
ASP_476@OD1	LYS_130@HZ2	LYS_130@NZ	0.0059	2.7653	158.4283
LEU_333@HB2	PHE_45@HB3	PHE_45@CB	0.0053	2.9425	143.589
SER_457@OG	LYS_46@HZ3	LYS_46@NZ	0.0053	2.891	151.9508
LEU_333@HD23	PHE_45@H	PHE_45@N	0.0052	2.8672	151.4475
ASN_427@OD1	LYS_54@HZ3	LYS_54@NZ	0.0048	2.8142	157.7675
ASP_472@OD1	LYS_130@HZ1	LYS_130@NZ	0.0046	2.8467	154.464
ASN_427@OD1	LYS_54@HZ1	LYS_54@NZ	0.0045	2.7991	153.8497
LEU_333@HG	PHE_42@HE1	PHE_42@CE1	0.0043	2.9516	143.577
ALA_428@O	TYR_37@HH	TYR_37@OH	0.004	2.8183	148.7259
PRO_466@HB3	ASP_96@HB3	ASP_96@CB	0.0037	2.9623	144.0466
GLU_317@OE2	ASN_107@HD21	ASN_107@ND2	0.0035	2.8222	153.9614
LEU_319@HD21	VAL_171@H	VAL_171@N	0.0033	2.815	155.9262
ASN_331@HD21	VAL_75@HG13	VAL_75@CG1	0.003	2.85	141.7809
ASN_427@HD21	SER_51@HB2	SER_51@CB	0.0027	2.8696	144.2883
GLN_464@HG2	GLY_49@HA3	GLY_49@CA	0.0027	2.9393	139.4896
GLU_327@OE1	TYR_176@HH	TYR_176@OH	0.0024	2.6819	166.529
ASN_427@HD21	SER_51@HG	SER_51@OG	0.0024	2.8665	143.9469
VAL_475@HG11	ASN_128@HD21	ASN_128@ND2	0.0023	2.7923	144.4682
GLU_317@HA	VAL_171@HG22	VAL_171@CG2	0.0022	2.92	140.3879
ALA_428@HA	THR_53@HG1	THR_53@OG1	0.0022	2.7893	142.2342
ASP_472@OD2	LYS_130@HZ2	LYS_130@NZ	0.0022	2.7822	152.305
ASP_472@OD2	ASN_128@HD22	ASN_128@ND2	0.0022	2.8082	161.9079
GLU_317@OE1	VAL_171@H	VAL_171@N	0.0021	2.8815	155.7281
ASN_331@HB2	LYS_46@HE3	LYS_46@CE	0.002	2.9421	147.061
VAL_475@HG11	ASN_128@HD22	ASN_128@ND2	0.002	2.8522	141.5941
ASN_331@OD1	LYS_46@HE3	LYS_46@CE	0.0019	2.9591	141.7372
PRO_466@HG3	ASP_96@HB3	ASP_96@CB	0.0019	2.9493	142.0084
GLN_316@HB3	GLY_170@HA3	GLY_170@CA	0.0018	2.9303	138.8393

LEU_319@HG	VAL_171@H	VAL_171@N	0.0017	2.8774	158.7462
ASP_472@OD1	LYS_130@HZ3	LYS_130@NZ	0.0017	2.8136	164.465
SER_457@HG	LYS_46@HZ1	LYS_46@NZ	0.0016	2.8916	146.0712
GLU_317@HA	VAL_171@HG23	VAL_171@CG2	0.0015	2.9379	142.0943
LEU_319@HD22	VAL_171@H	VAL_171@N	0.0015	2.8976	152.3946
LEU_333@HB3	PHE_42@HE1	PHE_42@CE1	0.0015	2.9549	148.5371
LEU_333@HD13	PHE_42@HE1	PHE_42@CE1	0.0015	2.9549	140.04
PRO_466@HB3	ASP_95@HB3	ASP_95@CB	0.0015	2.9671	140.5245
LEU_333@HD11	PHE_42@HE1	PHE_42@CE1	0.0014	2.9686	141.6854
THR_542@HG21	THR_83@HG1	THR_83@OG1	0.0014	2.7721	143.6129
GLU_317@HA	VAL_171@HG21	VAL_171@CG2	0.0013	2.9686	145.2795
LEU_319@HD23	VAL_171@H	VAL_171@N	0.0013	2.884	149.6015
SER_457@HB3	TYR_48@HE2	TYR_48@CE2	0.0013	2.9503	139.4367
GLN_464@HE21	LEU_58@HD23	LEU_58@CD2	0.0013	2.8596	144.8933
ASP_476@OD2	LYS_130@HZ1	LYS_130@NZ	0.0013	2.7489	157.2656
ASN_331@HA	LYS_46@HD2	LYS_46@CD	0.0012	2.9342	139.8101
ASN_331@HD21	VAL_75@HG11	VAL_75@CG1	0.0012	2.8643	140.1737
ASN_427@OD1	THR_53@H	THR_53@N	0.0012	2.9111	148.2271
VAL_475@HG12	ASN_128@H	ASN_128@N	0.0012	2.751	144.8835
VAL_475@HG23	ASN_128@HD22	ASN_128@ND2	0.0012	2.8926	142.5556
THR_542@HG23	THR_83@HG1	THR_83@OG1	0.0012	2.8627	142.9646
ASN_331@HA	LYS_46@HG3	LYS_46@CG	0.0011	2.964	143.6499
LEU_333@HD21	PHE_42@HZ	PHE_42@CZ	0.0011	2.9232	141.5742
LEU_333@HD21	PHE_42@HE1	PHE_42@CE1	0.0011	2.9527	139.503
LEU_333@HD22	TYR_37@HE1	TYR_37@CE1	0.0011	2.9652	141.9861
ALA_428@HA	THR_53@HB	THR_53@CB	0.0011	2.9593	144.4574
SER_457@HB3	TYR_48@HD2	TYR_48@CD2	0.0011	2.9123	138.4276
ASN_467@H	ASP_95@HB3	ASP_95@CB	0.0011	2.8942	147.5456
VAL_475@HG13	ASN_128@HD21	ASN_128@ND2	0.0011	2.8366	144.7026
GLU_317@OE2	VAL_171@H	VAL_171@N	0.001	2.9263	156.8533
ASN_331@HA	LYS_46@HE2	LYS_46@CE	0.001	2.9121	145.1363
LEU_333@HB2	PHE_42@HE1	PHE_42@CE1	0.001	2.9658	143.0629
LEU_333@HD22	PHE_45@HB3	PHE_45@CB	0.001	2.9496	139.9733
LEU_333@HD23	PHE_42@HE1	PHE_42@CE1	0.001	2.9506	138.0161
MET_426@O	LYS_54@HZ1	LYS_54@NZ	0.001	2.8714	158.8839
PRO_466@HA	ASP_96@HB3	ASP_96@CB	0.001	2.9614	146.7698
ASN_467@HD22	GLY_81@HA3	GLY_81@CA	0.001	2.921	145.4292
VAL_475@HG21	ASN_128@HD22	ASN_128@ND2	0.001	2.9064	141.0225
VAL_541@O	THR_83@HG1	THR_83@OG1	0.001	2.8889	151.712

Table 9.4: *Hydrogen bond analysis of S protein (BA.2)-ACE2 complex during the last 20 ns of MD simulation with S protein as acceptor and ACE2 as donor.*

#Acceptor	DonorH	Donor	Frac	Average Distance (Å)	Average Angles (°)
ASP_88@OD1	THR_542@HG1	THR_542@OG1	0.9647	2.6654	164.6703
ASP_88@OD1	THR_471@HG1	THR_471@OG1	0.5003	2.7392	166.4083
ASP_88@OD2	THR_471@HG1	THR_471@OG1	0.2685	2.6938	164.1908
PHE_39@O	GLN_316@HE22	GLN_316@NE2	0.2621	2.8512	158.2493
SER_162@O	ASN_515@HD22	ASN_515@ND2	0.1687	2.8529	158.212
ALA_40@O	ASN_314@HD22	ASN_314@ND2	0.1472	2.8452	158.2836
HIE_173@ND1	LYS_518@HZ2	LYS_518@NZ	0.0588	2.9133	155.668
TYR_163@O	ASN_515@HD22	ASN_515@ND2	0.0536	2.8694	152.5046
ALA_40@O	ASN_311@HD22	ASN_311@ND2	0.0472	2.8537	160.6247
HIE_173@ND1	LYS_518@HZ3	LYS_518@NZ	0.046	2.9081	154.2679
HIE_173@ND1	LYS_518@HZ1	LYS_518@NZ	0.0438	2.9004	154.6989
SER_162@OG	ASN_515@HD21	ASN_515@ND2	0.0407	2.8612	157.9923
PHE_42@O	ASN_311@HD21	ASN_311@ND2	0.0377	2.8201	151.4343
SER_76@O	ASN_331@HD22	ASN_331@ND2	0.0343	2.8913	144.8645
ALA_79@HB2	ASN_331@HD22	ASN_331@ND2	0.0258	2.8367	147.2984
ALA_79@HB1	ASN_331@HD22	ASN_331@ND2	0.0247	2.8314	144.9576
PRO_80@O	SER_457@HG	SER_457@OG	0.0236	2.7337	161.4115
ASN_38@O	ASN_314@HD21	ASN_314@ND2	0.0229	2.8625	155.6036
ALA_79@HB3	ASN_331@HD22	ASN_331@ND2	0.0211	2.8432	146.3181
ARG_161@HD3	GLY_514@HA2	GLY_514@CA	0.017	2.9234	146.0214
ALA_143@HA	ALA_478@HB3	ALA_478@CB	0.0161	2.9384	144.4056
ALA_143@HA	ALA_478@HB1	ALA_478@CB	0.0155	2.9378	145.621
ALA_143@HA	ALA_478@HB2	ALA_478@CB	0.0151	2.9436	145.4799
TYR_37@O	ASN_314@HD21	ASN_314@ND2	0.0147	2.8709	145.1977
GLY_114@O	ASN_515@HD22	ASN_515@ND2	0.0139	2.8622	161.1175
TYR_117@OH	ASN_515@HD22	ASN_515@ND2	0.0137	2.896	159.6331
ASP_95@OD1	GLN_464@HE22	GLN_464@NE2	0.0123	2.8582	160.1229
ASN_128@HD21	THR_471@HB	THR_471@CB	0.0116	2.8947	148.8492
GLY_81@O	ASN_467@HD21	ASN_467@ND2	0.0115	2.8401	156.3788
GLY_164@HA2	ASN_515@HD22	ASN_515@ND2	0.0107	2.8571	145.8386
ASN_85@HD22	LYS_540@HB2	LYS_540@CB	0.0105	2.8553	144.2317
PHE_43@HE1	GLU_327@HB3	GLU_327@CB	0.0101	2.9407	141.3841
GLU_74@OE2	LYS_540@HZ2	LYS_540@NZ	0.0092	2.8468	155.4526
TYR_157@HH	ASP_480@HB2	ASP_480@CB	0.0088	2.8974	148.1025
SER_162@OG	ASN_515@HD22	ASN_515@ND2	0.0088	2.9119	157.5968
ASN_85@OD1	THR_542@HG1	THR_542@OG1	0.0087	2.7628	159.4577
PHE_42@CE1	ASN_311@HD22	ASN_311@ND2	0.0083	2.9531	154.1856
LYS_46@HE2	ASN_331@HB3	ASN_331@CB	0.007	2.8815	145.7664
PHE_43@HB2	LEU_319@HG	LEU_319@CG	0.0067	2.9407	140.5247
THR_83@HB	ASP_544@HB2	ASP_544@CB	0.0067	2.9402	142.0697

PHE_42@HE2	ASN_314@HD21	ASN_314@ND2	0.0064	2.8436	146.1362
TYR_48@OH	SER_457@HG	SER_457@OG	0.0057	2.8545	160.667
PHE_43@HE1	GLY_324@HA2	GLY_324@CA	0.0055	2.9434	143.1251
ASN_128@HB3	ASP_472@HB2	ASP_472@CB	0.0047	2.9562	140.1362
ASN_85@HD22	LYS_540@HE3	LYS_540@CE	0.0045	2.8943	149.9352
TYR_176@HH	GLY_324@HA2	GLY_324@CA	0.0044	2.8966	148.3841
ARG_161@HH11	ASP_512@HB3	ASP_512@CB	0.0043	2.943	145.0297
ASN_85@HB2	LYS_540@HE2	LYS_540@CE	0.0041	2.9164	141.619
TYR_176@HH	LEU_319@HD12	LEU_319@CD1	0.0041	2.8176	143.5894
TYR_117@CD1	ASN_515@HD22	ASN_515@ND2	0.004	2.9534	153.4532
LYS_46@HD2	ASN_331@HB3	ASN_331@CB	0.0039	2.9492	140.8174
GLU_74@OE2	LYS_540@HZ1	LYS_540@NZ	0.0039	2.8028	154.9426
PRO_41@HB3	GLN_316@HG3	GLN_316@CG	0.0037	2.9481	140.938
TYR_48@OH	ASN_331@HD22	ASN_331@ND2	0.0035	2.893	142.4634
ASN_73@HA	PRO_323@HG3	PRO_323@CG	0.0035	2.9545	143.9954
GLN_82@HE21	ASN_331@HD22	ASN_331@ND2	0.0035	2.8868	146.9151
ASN_38@O	GLN_316@HE22	GLN_316@NE2	0.0034	2.8654	158.2105
GLY_84@HA2	ASP_544@HB2	ASP_544@CB	0.0033	2.9332	141.2042
GLU_74@OE1	LYS_540@HZ2	LYS_540@NZ	0.0032	2.7996	143.4653
GLU_74@OE2	LYS_540@HZ3	LYS_540@NZ	0.003	2.793	155.4852
VAL_171@HG21	LEU_320@H	LEU_320@N	0.0029	2.8822	149.4553
PHE_43@HZ	GLU_327@HG2	GLU_327@CG	0.0028	2.9483	142.953
TYR_117@HD1	ASN_515@HD22	ASN_515@ND2	0.0028	2.8795	145.197
TYR_117@HE1	ASN_515@HB3	ASN_515@CB	0.0028	2.9442	142.2482
ARG_161@HH12	GLY_514@H	GLY_514@N	0.0028	2.9381	140.71
TYR_121@OH	LYS_540@HZ2	LYS_540@NZ	0.0027	2.8832	149.6097
LEU_123@HD12	LYS_540@HG2	LYS_540@CG	0.0027	2.9421	140.4583
ASN_128@HB2	ASP_472@HB2	ASP_472@CB	0.0027	2.9453	139.4898
PHE_42@HE1	ASN_311@HD22	ASN_311@ND2	0.0026	2.916	149.8197
TYR_89@HH	VAL_541@HG22	VAL_541@CG2	0.0026	2.9128	145.6042
SER_76@HA	ASN_331@HD21	ASN_331@ND2	0.0025	2.8514	139.0097
LEU_123@HD11	LYS_540@HG2	LYS_540@CG	0.0025	2.9485	144.8126
HIE_173@CE1	LYS_518@HZ2	LYS_518@NZ	0.0025	2.9591	144.4559
ASN_128@HD21	THR_471@HG22	THR_471@CG2	0.0024	2.8687	143.4011
ASN_128@HD22	THR_471@HB	THR_471@CB	0.0024	2.8977	152.8809
VAL_171@HB	PRO_323@HD2	PRO_323@CD	0.0024	2.9267	141.9704
LEU_123@HD13	LYS_540@HG2	LYS_540@CG	0.0023	2.9422	141.1247
ASN_128@HD22	THR_471@HG1	THR_471@OG1	0.0023	2.8703	140.1777
PHE_42@O	ASN_311@HD22	ASN_311@ND2	0.0022	2.8269	152.2872
TYR_89@HH	VAL_541@HG23	VAL_541@CG2	0.0022	2.9224	149.4115
TYR_141@HE1	VAL_475@HB	VAL_475@CB	0.0022	2.9718	138.4731
GLY_164@HA3	ASN_515@HB3	ASN_515@CB	0.0022	2.929	145.8152
VAL_171@HG22	PRO_323@HD3	PRO_323@CD	0.0022	2.9493	141.9495
ASN_38@HA	ASN_314@HB2	ASN_314@CB	0.0021	2.9576	138.6894
TYR_89@HH	VAL_541@HG21	VAL_541@CG2	0.0021	2.9394	145.2132

TYR_89@HH	VAL_541@HB	VAL_541@CB	0.0021	2.9068	140.9454
LYS_108@HE2	GLN_316@HB2	GLN_316@CB	0.0021	2.8957	142.9185
ASN_128@HD21	THR_471@HG23	THR_471@CG2	0.0021	2.8476	143.2846
VAL_171@HG21	PRO_323@HD3	PRO_323@CD	0.0021	2.9411	142.5727
ASP_95@OD2	GLN_464@HE21	GLN_464@NE2	0.002	2.8227	158.8715
TYR_121@OH	LYS_540@HZ1	LYS_540@NZ	0.002	2.9035	147.9032
GLY_84@HA2	THR_542@HG21	THR_542@CG2	0.0019	2.9426	141.521
ARG_161@HG3	ASN_515@HA	ASN_515@CA	0.0019	2.931	146.0337
GLY_172@HA2	PRO_323@HG3	PRO_323@CG	0.0019	2.9494	140.0238
LYS_46@HG2	SER_332@HB2	SER_332@CB	0.0018	2.9186	140.9608
LYS_46@HE3	ASN_331@HB3	ASN_331@CB	0.0018	2.8957	140.2079
CYS_47@HB2	LEU_333@HB3	LEU_333@CB	0.0018	2.9544	144.8765
GLY_84@HA2	ASP_544@HB3	ASP_544@CB	0.0018	2.9513	138.6809
ASN_85@HB2	LYS_540@HE3	LYS_540@CE	0.0018	2.9101	141.0338
PHE_124@HE1	VAL_541@HG21	VAL_541@CG2	0.0018	2.9471	139.5552
ALA_143@HB1	ASP_480@HB3	ASP_480@CB	0.0018	2.9615	143.6659
VAL_171@HG13	PRO_323@HD2	PRO_323@CD	0.0018	2.932	141.855
HIE_173@CE1	LYS_518@HZ3	LYS_518@NZ	0.0018	2.955	143.983
LYS_46@HD3	ASN_331@HB3	ASN_331@CB	0.0017	2.9495	141.355
GLN_82@NE2	ASN_331@HD22	ASN_331@ND2	0.0017	2.9236	148.9167
VAL_171@HG11	PRO_323@HD2	PRO_323@CD	0.0017	2.9468	142.524
PRO_41@HA	GLN_316@HG3	GLN_316@CG	0.0016	2.9578	138.7748
LYS_46@HB3	SER_332@HA	SER_332@CA	0.0016	2.9375	137.2109
LYS_46@HD3	GLU_327@HG3	GLU_327@CG	0.0016	2.9478	139.3046
ASN_85@HB3	LYS_540@HE3	LYS_540@CE	0.0016	2.9437	141.9553
LYS_108@HE3	GLN_316@HB2	GLN_316@CB	0.0016	2.8805	147.2528
TYR_121@OH	LYS_540@HZ3	LYS_540@NZ	0.0016	2.889	149.4556
ASN_128@HB2	ASP_472@HA	ASP_472@CA	0.0016	2.9601	141.6737
VAL_75@HG13	GLU_327@HG2	GLU_327@CG	0.0015	2.9471	140.5195
ASP_95@OD2	GLN_464@HE22	GLN_464@NE2	0.0015	2.8596	157.3975

Table 9.5.*Hydrogen bond analysis of S protein (BA.2)-ACE2 complex during the last 20 ns of MD simulation with S protein as donor and ACE2 as acceptor.*

Acceptor	**DonorH**	**Donor**	**Frac**	**Average Distance (Å)**	**Average Angles (º)**
VAL_541@O	TYR_89@HH	TYR_89@OH	0.9229	2.7453	165.5502
TRP_479@O	TYR_141@HH	TYR_141@OH	0.8523	2.7577	165.5495
ASN_331@OD1	TYR_48@HH	TYR_48@OH	0.5694	2.7781	155.9643
ASP_480@OD1	ASN_155@HD22	ASN_155@ND2	0.4299	2.8563	165.0414
ASP_512@OD1	ARG_161@HH12	ARG_161@NH1	0.4242	2.7798	156.2918
ASP_472@OD2	ASN_128@H	ASN_128@N	0.2538	2.8659	164.1645
ASP_544@OD1	THR_83@HG1	THR_83@OG1	0.2297	2.7074	163.2369
GLU_327@OE2	LYS_46@HZ2	LYS_46@NZ	0.2001	2.7305	159.8604

GLU_327@OE1	LYS_46@HZ3	LYS_46@NZ	0.1975	2.7326	159.3155
ASP_472@OD1	ASN_128@H	ASN_128@N	0.1954	2.8657	161.9071
GLU_327@OE2	LYS_46@HZ3	LYS_46@NZ	0.1953	2.7282	158.1404
GLU_327@OE1	LYS_46@HZ1	LYS_46@NZ	0.1764	2.7224	158.4546
ASP_334@OD2	TYR_37@HH	TYR_37@OH	0.1652	2.6888	162.7179
GLU_337@OE2	PHE_45@H	PHE_45@N	0.1606	2.8781	157.8172
ASN_331@O	TYR_48@HH	TYR_48@OH	0.1573	2.7641	155.8226
GLU_317@OE2	ASN_105@H	ASN_105@N	0.1556	2.8427	165.4033
ASN_331@OD1	LYS_46@HZ1	LYS_46@NZ	0.1555	2.8224	155.0685
GLU_327@OE1	SER_76@HG	SER_76@OG	0.1478	2.6963	164.0958
ASP_512@O	ARG_161@HH11	ARG_161@NH1	0.1142	2.8459	147.1124
ASN_515@OD1	SER_162@H	SER_162@N	0.104	2.8644	158.9792
GLU_317@OE1	ASN_105@H	ASN_105@N	0.1021	2.8386	164.6936
GLU_327@OE2	LYS_46@HZ1	LYS_46@NZ	0.0976	2.7265	158.5452
ASP_472@OD2	ASN_128@HD21	ASN_128@ND2	0.0808	2.8236	163.1318
GLU_327@OE1	LYS_46@HZ2	LYS_46@NZ	0.0778	2.7222	157.7996
ASP_313@O	ASN_38@HD22	ASN_38@ND2	0.0709	2.8422	151.9465
ASN_331@OD1	LYS_46@HZ2	LYS_46@NZ	0.0703	2.8289	155.8814
ASN_331@OD1	LYS_46@HZ3	LYS_46@NZ	0.0696	2.8277	155.9213
GLN_316@O	LYS_108@HZ2	LYS_108@NZ	0.0584	2.8119	153.9518
THR_471@OG1	ASN_128@HD21	ASN_128@ND2	0.0459	2.875	159.1622
ASP_313@OD1	ASN_38@HD22	ASN_38@ND2	0.0425	2.8348	153.9379
GLU_317@OE1	LYS_108@HZ1	LYS_108@NZ	0.042	2.7905	157.4565
ASP_512@OD2	ARG_161@HH12	ARG_161@NH1	0.0406	2.7851	157.1577
GLN_316@O	LYS_108@HZ1	LYS_108@NZ	0.0389	2.8193	152.615
GLU_327@OE2	SER_76@HG	SER_76@OG	0.0385	2.6778	165.7468
ASP_480@OD2	ASN_155@HD22	ASN_155@ND2	0.0376	2.8213	163.0243
ASP_472@OD1	SER_127@HG	SER_127@OG	0.0364	2.6356	165.7015
GLU_337@OE1	PHE_45@H	PHE_45@N	0.036	2.9015	162.0898
GLN_316@O	LYS_108@HZ3	LYS_108@NZ	0.0347	2.8138	152.5818
GLU_317@OE1	LYS_108@HZ3	LYS_108@NZ	0.0322	2.797	157.085
GLU_317@OE1	LYS_108@HZ2	LYS_108@NZ	0.0262	2.7885	157.4804
LYS_540@HB2	ASN_85@HD22	ASN_85@ND2	0.0259	2.8187	146.9217
GLU_317@OE2	LYS_108@HZ2	LYS_108@NZ	0.0245	2.7841	157.9416
GLN_316@OE1	LYS_108@HZ3	LYS_108@NZ	0.0229	2.8066	153.6982
GLN_316@OE1	LYS_108@HZ1	LYS_108@NZ	0.0226	2.8089	155.1187
ASN_331@HD21	SER_76@HA	SER_76@CA	0.0218	2.9237	152.679
GLU_317@OE2	LYS_108@HZ1	LYS_108@NZ	0.0168	2.7941	155.7396
ASN_331@ND2	LYS_46@HZ1	LYS_46@NZ	0.0165	2.9079	148.1849
GLY_514@HA2	ARG_161@HD3	ARG_161@CD	0.0164	2.9166	143.37
GLU_317@OE2	LYS_108@HZ3	LYS_108@NZ	0.016	2.7927	153.9583
GLN_316@OE1	LYS_108@HZ2	LYS_108@NZ	0.0151	2.8211	155.0515
VAL_475@O	LYS_126@HZ3	LYS_126@NZ	0.0147	2.8358	157.536
ASN_515@OD1	SER_162@HG	SER_162@OG	0.0142	2.7313	156.5555
LEU_319@HD12	TYR_176@HH	TYR_176@OH	0.0133	2.7621	146.4185

ALA_478@HB1	ALA_143@HA	ALA_143@CA	0.0129	2.9414	148.1254
ASP_469@OD2	ASN_128@HD22	ASN_128@ND2	0.0127	2.8249	157.5205
ALA_478@HB3	ALA_143@HA	ALA_143@CA	0.0118	2.9479	147.9682
ASP_334@OD1	TYR_37@HH	TYR_37@OH	0.0113	2.7762	161.0213
ALA_478@HB2	ALA_143@HA	ALA_143@CA	0.0113	2.9431	148.5557
ASP_544@HB3	GLY_84@HA2	GLY_84@CA	0.0113	2.9453	143.1727
GLU_327@HB3	PHE_43@HE1	PHE_43@CE1	0.0111	2.9586	146.1893
VAL_475@O	LYS_126@HZ1	LYS_126@NZ	0.011	2.8406	157.8559
ASN_331@HB3	LYS_46@HE3	LYS_46@CE	0.0101	2.9208	146.1572
ALA_519@O	HIE_173@HE2	HIE_173@NE2	0.0086	2.9141	161.7022
THR_471@HG1	ASN_128@HD21	ASN_128@ND2	0.0084	2.8994	149.119
ASN_331@OD1	LYS_46@HE3	LYS_46@CE	0.0071	2.9644	143.3018
THR_471@HG23	ASN_128@HD21	ASN_128@ND2	0.0067	2.8375	146.0775
ASN_331@HB3	LYS_46@HE2	LYS_46@CE	0.0066	2.8803	148.0042
VAL_516@O	TYR_169@HH	TYR_169@OH	0.0066	2.8191	146.4795
ASP_334@OD2	LYS_54@HZ1	LYS_54@NZ	0.0056	2.8035	155.9428
GLN_316@HG3	PRO_41@HB3	PRO_41@CB	0.0055	2.954	141.3549
THR_471@HG22	ASN_128@HD21	ASN_128@ND2	0.0055	2.8199	146.2541
ASP_544@HB2	GLY_84@HA2	GLY_84@CA	0.0054	2.9282	141.0426
ASN_331@HD22	ALA_79@HB1	ALA_79@CB	0.0053	2.8313	142.4231
ASP_544@HB2	THR_83@HB	THR_83@CB	0.0053	2.9388	142.0956
THR_471@O	ASN_128@HD21	ASN_128@ND2	0.0051	2.8938	156.0918
ASN_515@OD1	TYR_117@HH	TYR_117@OH	0.0049	2.7572	159.6136
ASP_334@OD1	LYS_54@HZ1	LYS_54@NZ	0.0048	2.8147	157.7252
ASN_331@HD22	ALA_79@HB2	ALA_79@CB	0.0045	2.8618	143.5598
ASN_331@HD21	LYS_46@HZ3	LYS_46@NZ	0.0042	2.8723	148.867
ASN_331@HD21	LYS_46@HZ1	LYS_46@NZ	0.0042	2.8896	146.818
ASN_515@HB3	TYR_117@HE1	TYR_117@CE1	0.0041	2.9346	141.5653
LEU_319@HD13	TYR_176@HH	TYR_176@OH	0.0038	2.7926	146.2066
THR_471@HB	ASN_128@HD21	ASN_128@ND2	0.0037	2.7961	141.9411
GLU_327@HG2	PHE_43@HZ	PHE_43@CZ	0.0036	2.947	141.1631
ASN_331@HD22	ALA_79@HB3	ALA_79@CB	0.0036	2.8366	141.1552
ASN_515@HD22	GLY_164@HA2	GLY_164@CA	0.0036	2.856	141.3223
LEU_319@HG	PHE_43@HB2	PHE_43@CB	0.0035	2.9636	146.5823
ASP_512@O	ARG_161@HH22	ARG_161@NH2	0.0035	2.8645	153.4804
ASP_480@HB2	TYR_157@HH	TYR_157@OH	0.0034	2.8303	142.5693
ASN_515@HD22	SER_162@HB2	SER_162@CB	0.0034	2.9031	145.6085
ASN_515@O	TYR_117@HH	TYR_117@OH	0.0034	2.8225	155.896
VAL_475@HG22	SER_127@HA	SER_127@CA	0.0033	2.9419	139.9848
VAL_475@HG23	SER_127@HA	SER_127@CA	0.0033	2.9301	140.8669
ASP_472@HB2	ASN_128@HB3	ASN_128@CB	0.0032	2.9472	139.4292
ASP_512@OD1	ARG_161@HH11	ARG_161@NH1	0.0032	2.7606	156.1972
ASN_515@HD21	SER_162@HB2	SER_162@CB	0.0032	2.9292	143.4778
CYS_521@HG	HIE_173@HE2	HIE_173@NE2	0.0032	2.8284	144.7035
LYS_540@HE3	ASN_85@HB2	ASN_85@CB	0.0032	2.9034	142.629

ASN_515@O	ARG_166@HH22	ARG_166@NH2	0.0031	2.843	151.23
LYS_540@HB3	ASN_85@HD22	ASN_85@ND2	0.0031	2.8345	140.8462
CYS_521@HG	HIE_173@HE1	HIE_173@CE1	0.003	2.8487	149.6786
ASN_314@HD21	PHE_42@HE2	PHE_42@CE2	0.0028	2.8857	140.0951
ASN_331@CG	TYR_48@HH	TYR_48@OH	0.0027	2.9598	139.2511
VAL_541@HB	TYR_89@HH	TYR_89@OH	0.0027	2.8551	144.9296
VAL_475@O	LYS_126@HZ2	LYS_126@NZ	0.0026	2.8457	159.9295
ASP_480@HB3	ASN_155@HD22	ASN_155@ND2	0.0026	2.8656	142.6375
LYS_540@HE2	ASN_85@HB2	ASN_85@CB	0.0026	2.9101	144.7857
VAL_541@HG21	PHE_124@HE1	PHE_124@CE1	0.0026	2.9613	140.2385
ASN_331@ND2	LYS_46@HZ2	LYS_46@NZ	0.0025	2.9126	148.913
VAL_516@O	ARG_166@HH21	ARG_166@NH2	0.0025	2.8446	148.143
VAL_516@O	TYR_117@HH	TYR_117@OH	0.0025	2.8024	157.567
LYS_540@HG2	LEU_123@HD13	LEU_123@CD1	0.0025	2.9483	140.1259
THR_542@HG23	ASN_85@HD22	ASN_85@ND2	0.0025	2.853	141.854
GLU_337@OE1	LYS_46@H	LYS_46@N	0.0024	2.9464	157.0218
PRO_323@HD2	VAL_171@HB	VAL_171@CB	0.0023	2.9421	140.7465
PRO_323@HD3	VAL_171@HG21	VAL_171@CG2	0.0023	2.9389	140.2554
PRO_323@HG3	ASN_73@HA	ASN_73@CA	0.0023	2.9461	143.7192
PRO_323@HG3	GLY_172@HA2	GLY_172@CA	0.0023	2.9467	143.8965
ASN_331@ND2	LYS_46@HZ3	LYS_46@NZ	0.0023	2.914	148.8365
THR_471@HG21	ASN_128@HD21	ASN_128@ND2	0.0023	2.8145	147.0784
ASP_469@OD1	ASN_128@HD22	ASN_128@ND2	0.0022	2.9194	160.1775
ASP_544@HB2	THR_83@HG1	THR_83@OG1	0.0022	2.7592	145.1275
ASN_331@HB3	LYS_46@HD2	LYS_46@CD	0.0021	2.9601	143.9109
VAL_475@HG21	SER_127@HA	SER_127@CA	0.0021	2.9566	141.9469
ASN_515@HB3	GLY_164@HA3	GLY_164@CA	0.0021	2.9421	145.9427
LYS_540@HG2	LEU_123@HD11	LEU_123@CD1	0.0021	2.9558	141.3499
MET_543@HB3	THR_83@HB	THR_83@CB	0.0021	2.9479	141.1959
GLN_316@HB2	LYS_108@HE2	LYS_108@CE	0.002	2.8702	143.3183
LEU_319@HD11	TYR_176@HH	TYR_176@OH	0.002	2.7641	152.6718
ASN_331@HD21	LYS_46@HZ2	LYS_46@NZ	0.002	2.8911	150.1725
SER_457@OG	GLN_82@HE21	GLN_82@NE2	0.002	2.9051	161.4428
THR_471@HB	ASN_128@HD22	ASN_128@ND2	0.002	2.8187	144.1972
LYS_540@HG2	LEU_123@HD12	LEU_123@CD1	0.002	2.9481	141.1535
GLN_316@HB2	LYS_108@HE3	LYS_108@CE	0.0019	2.8812	144.937
GLY_324@HA2	TYR_176@HH	TYR_176@OH	0.0019	2.8929	141.007
GLU_327@HG3	LYS_46@HD3	LYS_46@CD	0.0018	2.9617	141.4255
THR_471@HG21	ASN_128@HD22	ASN_128@ND2	0.0018	2.8435	142.66
VAL_475@HG12	TYR_89@HE2	TYR_89@CE2	0.0018	2.9595	142.7604
ASN_515@HD22	TYR_117@HD1	TYR_117@CD1	0.0018	2.8749	145.9126
VAL_541@HG23	PHE_124@HE1	PHE_124@CE1	0.0018	2.9592	142.2585
THR_542@HG21	GLY_84@HA2	GLY_84@CA	0.0018	2.9511	146.3151
ASN_331@HD22	LYS_46@HZ1	LYS_46@NZ	0.0017	2.9212	144.4266
ASP_472@HA	ASN_128@HB2	ASN_128@CB	0.0017	2.9513	145.8543

VAL_475@HB	TYR_141@HE1	TYR_141@CE1	0.0017	2.9718	141.9103
ASP_476@OD2	LYS_126@HZ3	LYS_126@NZ	0.0017	2.7775	157.6579
THR_542@HG22	GLY_84@HA2	GLY_84@CA	0.0017	2.9375	145.8437
LEU_319@HG	PHE_43@HD1	PHE_43@CD1	0.0016	2.9457	139.9284
ASP_472@HB2	ASN_128@HB2	ASN_128@CB	0.0016	2.9578	139.5966
ASN_515@OD1	ARG_166@HH22	ARG_166@NH2	0.0016	2.8405	147.9694
THR_542@HG22	ASN_85@HD22	ASN_85@ND2	0.0016	2.8576	142.4397
ASP_544@OD2	THR_83@HG1	THR_83@OG1	0.0016	2.6518	164.797
ASN_331@OD1	GLN_82@HE21	GLN_82@NE2	0.0015	2.8738	150.7245
THR_471@HG23	ASN_128@HD22	ASN_128@ND2	0.0015	2.8076	147.2106
VAL_541@HG22	PHE_124@HE1	PHE_124@CE1	0.0015	2.9436	144.8802
GLN_316@HE21	PRO_41@HA	PRO_41@CA	0.0014	2.9288	144.4343
LYS_518@HE2	GLY_164@HA3	GLY_164@CA	0.0014	2.9271	146.5358
PRO_315@O	LYS_108@HZ3	LYS_108@NZ	0.0013	2.8377	157.3589
GLN_316@HG3	LYS_108@HE3	LYS_108@CE	0.0013	2.8796	147.2
GLN_316@HG3	PRO_41@HA	PRO_41@CA	0.0013	2.9428	138.2682
LEU_319@HD13	PHE_43@HB2	PHE_43@CB	0.0013	2.9194	141.3627
THR_471@HG1	ASN_128@HD22	ASN_128@ND2	0.0013	2.8972	139.5625
LEU_320@H	VAL_171@HG21	VAL_171@CG2	0.0012	2.87	151.5885
PRO_323@HD3	VAL_171@HG23	VAL_171@CG2	0.0012	2.9287	144.7265
VAL_475@HB	LYS_126@HA	LYS_126@CA	0.0012	2.9514	142.3197
VAL_475@HG13	TYR_89@HE2	TYR_89@CE2	0.0012	2.9636	140.2939
LEU_319@HD12	PHE_43@HB2	PHE_43@CB	0.0011	2.9625	142.0874
ILE_328@HG12	ALA_44@HB2	ALA_44@CB	0.0011	2.9626	140.1355
ASN_331@HB3	LYS_46@HD3	LYS_46@CD	0.0011	2.9353	142.4427
SER_332@HB2	LYS_46@HG2	LYS_46@CG	0.0011	2.9385	147.4037
LYS_540@HD2	ASN_85@HB2	ASN_85@CB	0.0011	2.9478	139.3069
GLU_317@HB3	PHE_42@H	PHE_42@N	0.001	2.9285	142.3313
ASN_331@HD22	TYR_48@HH	TYR_48@OH	0.001	2.897	141.3542
ASP_472@HB2	ASN_128@HD21	ASN_128@ND2	0.001	2.74	146.5143
VAL_475@HG11	TYR_89@HE2	TYR_89@CE2	0.001	2.9712	143.3908
THR_542@HG1	GLY_84@H	GLY_84@N	0.001	2.873	140.4149

9.4.1.4. Determination of the interface interactions of the S protein (BA.1)-ACE2 and (S protein (BA.2)-ACE2 complexes.

An interface area is usually defined as a region where two sets of proteins come in contact with each other. Surface residues with large surface regions accessible to the solvent available usually characterize them. The interface statistics for the S protein (BA.1)-ACE2 and S protein (BA.2)-ACE2 complexes were obtained upon the submission of the corresponding lowest energy structure extracted from the 50 ns MD simulation trajectory using RMSD clustering algorithm to the PDBsum server. The interface statistics for both the complexes have been summarised in **Table 9.6.**

Table 9.6. *Interface statistics for the S protein (BA.1)-ACE2 and S protein (BA.2)-ACE2 complexes.*

Complex System	Chain	No. of Interface Residues	Interface area(Å^2)	No. of Salt Bridges	No. of Disulphide Bonds	No. of Hydrogen bonds	No. of Non-Bonded Contacts
S Protein (BA1-ACE2)	ACE2	36	1479	3	-	19	246
	SPIKE (BA.1)	31	1574				
S Protein (BA2-ACE2)	ACE2	42	2066	4	-	18	255
	SPIKE (BA.2)	46	2012				

The summarized intermolecular interactions between S protein and ACE2 in S protein (BA.1)-ACE2 and S protein (BA.2)-ACE2 complexes at the residue levels were shown in **Figure 9.11.**

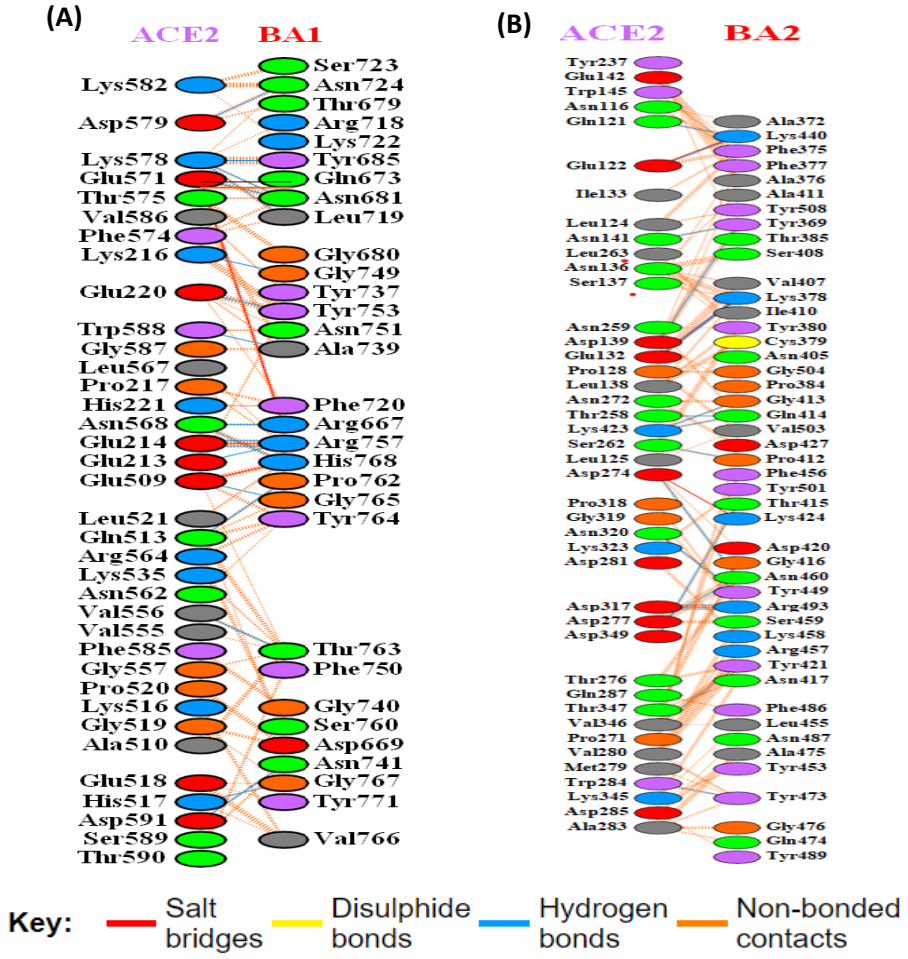

Figure 9.11. *Intermolecular interactions at residue level between ACE2 and S protein in* ***(A)*** *S protein (BA.1)-ACE2 and* ***(B)*** *S protein (BA.2)-ACE2 complex.*

The detailed contributions of each interface residue stabilizing the BA.1 and BA.2 complexes were summarized in **Table 9.7-9.12**. The total number of interface residues in the S protein (BA.1)-ACE2 and S protein (BA.2)-ACE2 complexes were found to be sixty-seven and eighty-eight respectively.

In the S protein (BA.1)-ACE2 complex, the interface area for the S protein chain and the ACE2 chain involved in the interaction was observed to be 1479Å^2 and 1574Å^2 respectively, while in the S protein (BA.2)-ACE2 complex, the S protein chain and the ACE2 chain involved in the interaction was observed to be 2066 Å^2 and 2012 Å^2 respectively. Both the BA.1and BA.2 complexes were stabilized by molecular interactions like salt bridges, hydrogen bonding, and non-bonded contacts. From **Table 9.7-9.12**, we can see the presence of two hundred and forty-six non-bonded contacts, three salt bridge and nineteen hydrogen bonds at the interface of S protein and ACE2 in the S protein (BA.1)-ACE2 complex. However, at the interface of S protein and ACE2 in the S protein (BA.2)-ACE2 complex, we observed two hundred and fifty-five non-bonded contacts, four salt bridge and eighteen hydrogen bonds. Overall, we see the number of intermolecular interactions and the interface area shared by S protein and ACE2 in forming complex is larger in BA.2 complex than in the BA.1type complex. Therefore, the stability of BA.2 complex was found to be higher than the BA.1 type complex.

Table 9.7. *List of atom-atom interactions (Hydrogen bonds) across protein-ligand interface in ACE2(chain A)-Spike Protein (Chain B) (BA.1variant) complex from PDBsum server*

Sl. No.	Atom no.	Atom name	Res name	Res no.	Chain Id	Hydrogen bonds	Atom no.	Atom name	Residue name	Res no.	Chain Id	Distance (Å)
1	2136	O	GLU	231	A	<-->	7489	NH2	ARG	493	B	3.29
2	2146	O	GLU	232	A	<-->	7486	NH1	ARG	493	B	3.02
3	2143	OE1	GLU	232	A	<-->	7486	NH1	ARG	493	B	2.67
4	2163	NZ	LYS	234	A	<-->	7404	O	GLY	485	B	3.02
5	2206	OE2	GLU	238	A	<-->	7445	OH	TYR	489	B	2.54
6	5047	O	GLU	527	A	<-->	7566	N	GLY	501	B	3.27
7	5077	NE2	GLN	531	A	<-->	7542	O	PRO	498	B	2.77
8	5118	O	HIS	535	A	<-->	7579	N	GLY	503	B	3.31
9	5486	O	VAL	574	A	<-->	7547	OG1	THR	499	B	2.75
10	5602	O	ASN	586	A	<-->	6598	NH2	ARG	403	B	3.07
11	5597	OD1	ASN	586	A	<-->	7589	ND1	HIS	504	B	2.65
12	5636	OE2	GLU	589	A	<-->	6659	NE2	GLN	409	B	3
13	5636	OE2	GLU	589	A	<-->	6723	ND2	ASN	417	B	2.76
14	5713	O	LYS	596	A	<-->	6762	OH	TYR	421	B	2.82
15	5708	NZ	LYS	596	A	<-->	6722	OD1	ASN	417	B	2.66

16	5708	NZ	LYS	596	A	<-->	7111	O	LEU	455	B	2.72
17	5719	OD1	ASP	597	A	<-->	7168	ND2	ASN	460	B	2.66
18	5803	N	TRP	606	A	<-->	7326	O	ALA	475	B	3.22
19	5842	OD2	ASP	609	A	<-->	7338	ND2	ASN	477	B	2.74

Table 9.8. *List of atom-atom interactions (non-bonded contacts) across protein-ligand interface in ACE2(chain A)-Spike Protein (Chain B) (BA.1variant) complex from PDBsum server*

Sl. No.	Atom no.	Atom name	Residue name	Residue no.	Chain Id	Non-bonded contacts	Atom no.	Atom name	Residue name	Residue no.	Chain Id	Distance (Å)
1	2136	O	GLU	231	A	<-->	7489	NH2	ARG	493	B	3.29
2	2133	OE1	GLU	231	A	<-->	7441	CD2	TYR	489	B	3.49
3	2133	OE1	GLU	231	A	<-->	7443	CE2	TYR	489	B	3.31
4	2139	CA	GLU	232	A	<-->	7485	CZ	ARG	493	B	3.69
5	2139	CA	GLU	232	A	<-->	7486	NH1	ARG	493	B	3.33
6	2139	CA	GLU	232	A	<-->	7489	NH2	ARG	493	B	3.4
7	2145	C	GLU	232	A	<-->	7486	NH1	ARG	493	B	3.59
8	2146	O	GLU	232	A	<-->	7485	CZ	ARG	493	B	3.78
9	2146	O	GLU	232	A	<-->	7486	NH1	ARG	493	B	3.02
10	2146	O	GLU	232	A	<-->	7489	NH2	ARG	493	B	3.63
11	2140	CB	GLU	232	A	<-->	7486	NH1	ARG	493	B	3.45
12	2141	CG	GLU	232	A	<-->	7485	CZ	ARG	493	B	3.83
13	2141	CG	GLU	232	A	<-->	7486	NH1	ARG	493	B	3.5
14	2142	CD	GLU	232	A	<-->	7486	NH1	ARG	493	B	3.49
15	2143	OE1	GLU	232	A	<-->	7482	CD	ARG	493	B	3.24
16	2143	OE1	GLU	232	A	<-->	7483	NE	ARG	493	B	3.57
17	2143	OE1	GLU	232	A	<-->	7485	CZ	ARG	493	B	3.35
18	2143	OE1	GLU	232	A	<-->	7486	NH1	ARG	493	B	2.67
19	2159	CB	LYS	234	A	<-->	7443	CE2	TYR	489	B	3.85
20	2159	CB	LYS	234	A	<-->	7444	CZ	TYR	489	B	3.76
21	2159	CB	LYS	234	A	<-->	7445	OH	TYR	489	B	3.4
22	2162	CE	LYS	234	A	<-->	7443	CE2	TYR	489	B	3.43
23	2162	CE	LYS	234	A	<-->	7444	CZ	TYR	489	B	3.7
24	2162	CE	LYS	234	A	<-->	7445	OH	TYR	489	B	3.05
25	2163	NZ	LYS	234	A	<-->	7404	O	GLY	485	B	3.02
26	2163	NZ	LYS	234	A	<-->	7443	CE2	TYR	489	B	3.19
27	2163	NZ	LYS	234	A	<-->	7444	CZ	TYR	489	B	3.85
28	2163	NZ	LYS	234	A	<-->	7445	OH	TYR	489	B	3.6
29	2170	CA	PRO	235	A	<-->	7121	CZ	PHE	456	B	3.84
30	2171	CB	PRO	235	A	<-->	7120	CE2	PHE	456	B	3.58
31	2171	CB	PRO	235	A	<-->	7121	CZ	PHE	456	B	3.46
32	2172	CG	PRO	235	A	<-->	7120	CE2	PHE	456	B	3.85

33	2172	CG	PRO	235	A	<-->	7489	NH2	ARG	493	B	3.34
34	2173	CD	PRO	235	A	<-->	7489	NH2	ARG	493	B	3.85
35	2204	CD	GLU	238	A	<-->	7324	CB	ALA	475	B	3.89
36	2204	CD	GLU	238	A	<-->	7442	CE1	TYR	489	B	3.35
37	2204	CD	GLU	238	A	<-->	7444	CZ	TYR	489	B	3.78
38	2204	CD	GLU	238	A	<-->	7445	OH	TYR	489	B	3.35
39	2205	OE1	GLU	238	A	<-->	7121	CZ	PHE	456	B	3.61
40	2205	OE1	GLU	238	A	<-->	7440	CD1	TYR	489	B	3.89
41	2205	OE1	GLU	238	A	<-->	7442	CE1	TYR	489	B	3.09
42	2205	OE1	GLU	238	A	<-->	7444	CZ	TYR	489	B	3.88
43	2205	OE1	GLU	238	A	<-->	7445	OH	TYR	489	B	3.89
44	2206	OE2	GLU	238	A	<-->	7324	CB	ALA	475	B	3.69
45	2206	OE2	GLU	238	A	<-->	7419	CA	ASN	487	B	3.66
46	2206	OE2	GLU	238	A	<-->	7442	CE1	TYR	489	B	2.97
47	2206	OE2	GLU	238	A	<-->	7444	CZ	TYR	489	B	3.17
48	2206	OE2	GLU	238	A	<-->	7445	OH	TYR	489	B	2.54
49	2215	CD2	HIS	239	A	<-->	7119	CE1	PHE	456	B	3.77
50	2217	NE2	HIS	239	A	<-->	7119	CE1	PHE	456	B	3.37
51	5047	O	GLU	527	A	<-->	7551	O	THR	499	B	3.9
52	5047	O	GLU	527	A	<-->	7566	N	GLY	501	B	3.27
53	5042	CG	GLU	527	A	<-->	7588	CG	HIS	504	B	3.87
54	5042	CG	GLU	527	A	<-->	7591	CD2	HIS	504	B	3.7
55	5042	CG	GLU	527	A	<-->	7593	NE2	HIS	504	B	3.81
56	5043	CD	GLU	527	A	<-->	7557	CD1	TYR	500	B	3.82
57	5043	CD	GLU	527	A	<-->	7588	CG	HIS	504	B	3.71
58	5043	CD	GLU	527	A	<-->	7589	ND1	HIS	504	B	3.74
59	5045	OE2	GLU	527	A	<-->	7555	CB	TYR	500	B	3.26
60	5045	OE2	GLU	527	A	<-->	7556	CG	TYR	500	B	3.42
61	5045	OE2	GLU	527	A	<-->	7557	CD1	TYR	500	B	3.19
62	5045	OE2	GLU	527	A	<-->	7587	CB	HIS	504	B	3.37
63	5045	OE2	GLU	527	A	<-->	7588	CG	HIS	504	B	3.43
64	5045	OE2	GLU	527	A	<-->	7589	ND1	HIS	504	B	3.76
65	5048	N	ALA	528	A	<-->	7551	O	THR	499	B	3.78
66	5050	CA	ALA	528	A	<-->	7551	O	THR	499	B	2.96
67	5052	C	ALA	528	A	<-->	7551	O	THR	499	B	3.89
68	5053	O	ALA	528	A	<-->	7551	O	THR	499	B	3.84
69	5051	CB	ALA	528	A	<-->	7551	O	THR	499	B	3.38
70	5072	CA	GLN	531	A	<-->	7568	CA	GLY	501	B	3.67
71	5073	CB	GLN	531	A	<-->	7550	C	THR	499	B	3.74
72	5073	CB	GLN	531	A	<-->	7551	O	THR	499	B	3.58
73	5073	CB	GLN	531	A	<-->	7564	C	TYR	500	B	3.58
74	5073	CB	GLN	531	A	<-->	7565	O	TYR	500	B	3.58
75	5073	CB	GLN	531	A	<-->	7566	N	GLY	501	B	3.8
76	5074	CG	GLN	531	A	<-->	7542	O	PRO	498	B	3.71

77	5074	CG	GLN	531	A	<-->	7550	C	THR	499	B	3.67
78	5074	CG	GLN	531	A	<-->	7552	N	TYR	500	B	3.83
79	5074	CG	GLN	531	A	<-->	7564	C	TYR	500	B	3.82
80	5074	CG	GLN	531	A	<-->	7565	O	TYR	500	B	3.37
81	5075	CD	GLN	531	A	<-->	7542	O	PRO	498	B	3.67
82	5075	CD	GLN	531	A	<-->	7545	CA	THR	499	B	3.74
83	5077	NE2	GLN	531	A	<-->	7541	C	PRO	498	B	3.68
84	5077	NE2	GLN	531	A	<-->	7542	O	PRO	498	B	2.77
85	5077	NE2	GLN	531	A	<-->	7545	CA	THR	499	B	3.35
86	5096	CA	LYS	534	A	<-->	7576	CG2	VAL	502	B	3.47
87	5105	C	LYS	534	A	<-->	7576	CG2	VAL	502	B	3.62
88	5106	O	LYS	534	A	<-->	7576	CG2	VAL	502	B	3.84
89	5097	CB	LYS	534	A	<-->	7576	CG2	VAL	502	B	3.75
90	5118	O	HIS	535	A	<-->	7571	N	VAL	502	B	3.58
91	5118	O	HIS	535	A	<-->	7579	N	GLY	503	B	3.31
92	5124	CD	GLU	536	A	<-->	7574	CB	VAL	502	B	3.49
93	5124	CD	GLU	536	A	<-->	7575	CG1	VAL	502	B	3.63
94	5125	OE1	GLU	536	A	<-->	7574	CB	VAL	502	B	3.35
95	5125	OE1	GLU	536	A	<-->	7575	CG1	VAL	502	B	3.5
96	5125	OE1	GLU	536	A	<-->	7579	N	GLY	503	B	3.88
97	5125	OE1	GLU	536	A	<-->	7626	OH	TYR	507	B	3.41
98	5126	OE2	GLU	536	A	<-->	7574	CB	VAL	502	B	3.36
99	5126	OE2	GLU	536	A	<-->	7575	CG1	VAL	502	B	3.13
100	5126	OE2	GLU	536	A	<-->	7576	CG2	VAL	502	B	3.71
101	5129	N	GLY	537	A	<-->	7581	CA	GLY	503	B	3.86
102	5132	C	GLY	537	A	<-->	6612	CG	ASP	405	B	3.63
103	5132	C	GLY	537	A	<-->	6613	OD1	ASP	405	B	3.22
104	5133	O	GLY	537	A	<-->	6612	CG	ASP	405	B	3.58
105	5133	O	GLY	537	A	<-->	6613	OD1	ASP	405	B	2.99
106	5133	O	GLY	537	A	<-->	6614	OD2	ASP	405	B	3.74
107	5134	N	PRO	538	A	<-->	6612	CG	ASP	405	B	3.59
108	5134	N	PRO	538	A	<-->	6613	OD1	ASP	405	B	3.65
109	5134	N	PRO	538	A	<-->	6614	OD2	ASP	405	B	3.72
110	5135	CA	PRO	538	A	<-->	6612	CG	ASP	405	B	3.52
111	5135	CA	PRO	538	A	<-->	6614	OD2	ASP	405	B	3.14
112	5139	C	PRO	538	A	<-->	6614	OD2	ASP	405	B	3.78
113	5141	N	LEU	539	A	<-->	6614	OD2	ASP	405	B	3.38
114	5144	CB	LEU	539	A	<-->	7592	CE1	HIS	504	B	3.46
115	5144	CB	LEU	539	A	<-->	7593	NE2	HIS	504	B	3.54
116	5146	CD1	LEU	539	A	<-->	7593	NE2	HIS	504	B	3.42
117	5275	CE	LYS	553	A	<-->	7549	CG2	THR	499	B	3.71
118	5276	NZ	LYS	553	A	<-->	7549	CG2	THR	499	B	3.15
119	5478	O	VAL	573	A	<-->	7549	CG2	THR	499	B	3.61
120	5485	C	VAL	574	A	<-->	7546	CB	THR	499	B	3.65

121	5485	C	VAL	574	A	<-->	7547	OG1	THR	499	B	3.45
122	5486	O	VAL	574	A	<-->	7546	CB	THR	499	B	3.18
123	5486	O	VAL	574	A	<-->	7547	OG1	THR	499	B	2.75
124	5487	N	GLY	575	A	<-->	7547	OG1	THR	499	B	3.73
125	5489	CA	GLY	575	A	<-->	7547	OG1	THR	499	B	3.37
126	5537	ND2	ASN	580	A	<-->	7562	OH	TYR	500	B	3.2
127	5554	CG	ARG	582	A	<-->	7519	CB	SER	496	B	3.58
128	5556	NE	ARG	582	A	<-->	7523	O	SER	496	B	3.85
129	5556	NE	ARG	582	A	<-->	7519	CB	SER	496	B	3.61
130	5562	NH2	ARG	582	A	<-->	7523	O	SER	496	B	3.67
131	5562	NH2	ARG	582	A	<-->	7556	CG	TYR	500	B	3.54
132	5562	NH2	ARG	582	A	<-->	7557	CD1	TYR	500	B	3.5
133	5562	NH2	ARG	582	A	<-->	7558	CD2	TYR	500	B	3.81
134	5562	NH2	ARG	582	A	<-->	7559	CE1	TYR	500	B	3.75
135	5588	CD1	LEU	585	A	<-->	7486	NH1	ARG	493	B	3.23
136	5602	O	ASN	586	A	<-->	6598	NH2	ARG	403	B	3.07
137	5596	CG	ASN	586	A	<-->	7589	ND1	HIS	504	B	3.45
138	5596	CG	ASN	586	A	<-->	7592	CE1	HIS	504	B	3.77
139	5597	OD1	ASN	586	A	<-->	6592	NE	ARG	403	B	3.25
140	5597	OD1	ASN	586	A	<-->	6594	CZ	ARG	403	B	3.19
141	5597	OD1	ASN	586	A	<-->	6598	NH2	ARG	403	B	3.13
142	5597	OD1	ASN	586	A	<-->	7588	CG	HIS	504	B	3.89
143	5597	OD1	ASN	586	A	<-->	7589	ND1	HIS	504	B	2.65
144	5597	OD1	ASN	586	A	<-->	7592	CE1	HIS	504	B	3.15
145	5598	ND2	ASN	586	A	<-->	7589	ND1	HIS	504	B	3.59
146	5598	ND2	ASN	586	A	<-->	7592	CE1	HIS	504	B	3.57
147	5638	O	GLU	589	A	<-->	6723	ND2	ASN	417	B	3.86
148	5632	CB	GLU	589	A	<-->	6595	NH1	ARG	403	B	3.67
149	5632	CB	GLU	589	A	<-->	6598	NH2	ARG	403	B	3.52
150	5633	CG	GLU	589	A	<-->	6595	NH1	ARG	403	B	3.23
151	5633	CG	GLU	589	A	<-->	6723	ND2	ASN	417	B	3.44
152	5634	CD	GLU	589	A	<-->	6595	NH1	ARG	403	B	3.83
153	5634	CD	GLU	589	A	<-->	6659	NE2	GLN	409	B	3.45
154	5634	CD	GLU	589	A	<-->	6723	ND2	ASN	417	B	3.49
155	5635	OE1	GLU	589	A	<-->	6598	NH2	ARG	403	B	3.89
156	5635	OE1	GLU	589	A	<-->	6659	NE2	GLN	409	B	3.19
157	5636	OE2	GLU	589	A	<-->	6659	NE2	GLN	409	B	3
158	5636	OE2	GLU	589	A	<-->	6717	N	ASN	417	B	3.58
159	5636	OE2	GLU	589	A	<-->	6720	CB	ASN	417	B	3.12
160	5636	OE2	GLU	589	A	<-->	6721	CG	ASN	417	B	3.41
161	5636	OE2	GLU	589	A	<-->	6723	ND2	ASN	417	B	2.76
162	5661	CD2	PHE	592	A	<-->	6722	OD1	ASN	417	B	3.5
163	5661	CD2	PHE	592	A	<-->	6723	ND2	ASN	417	B	3.46
164	5663	CE2	PHE	592	A	<-->	6722	OD1	ASN	417	B	3.66

165	5663	CE2	PHE	592	A	<-->	7107	CG	LEU	455	B	3.66
166	5663	CE2	PHE	592	A	<-->	7108	CD1	LEU	455	B	3.53
167	5670	CB	THR	593	A	<-->	6712	N	GLY	416	B	3.76
168	5670	CB	THR	593	A	<-->	6714	CA	GLY	416	B	3.06
169	5670	CB	THR	593	A	<-->	6715	C	GLY	416	B	3.62
170	5670	CB	THR	593	A	<-->	6717	N	ASN	417	B	3.66
171	5671	OG1	THR	593	A	<-->	6714	CA	GLY	416	B	3.88
172	5673	CG2	THR	593	A	<-->	6714	CA	GLY	416	B	3.34
173	5673	CG2	THR	593	A	<-->	6715	C	GLY	416	B	3.75
174	5673	CG2	THR	593	A	<-->	6717	N	ASN	417	B	3.32
175	5712	C	LYS	596	A	<-->	6762	OH	TYR	421	B	3.63
176	5713	O	LYS	596	A	<-->	6759	CE1	TYR	421	B	3.76
177	5713	O	LYS	596	A	<-->	6761	CZ	TYR	421	B	3.6
178	5713	O	LYS	596	A	<-->	6762	OH	TYR	421	B	2.82
179	5713	O	LYS	596	A	<-->	7167	OD1	ASN	460	B	3.82
180	5704	CB	LYS	596	A	<-->	6759	CE1	TYR	421	B	3.85
181	5704	CB	LYS	596	A	<-->	6761	CZ	TYR	421	B	3.69
182	5704	CB	LYS	596	A	<-->	6762	OH	TYR	421	B	3.87
183	5706	CD	LYS	596	A	<-->	6760	CE2	TYR	421	B	3.86
184	5706	CD	LYS	596	A	<-->	7111	O	LEU	455	B	3.17
185	5707	CE	LYS	596	A	<-->	6722	OD1	ASN	417	B	3.14
186	5707	CE	LYS	596	A	<-->	6756	CG	TYR	421	B	3.71
187	5707	CE	LYS	596	A	<-->	6758	CD2	TYR	421	B	3.68
188	5707	CE	LYS	596	A	<-->	7111	O	LEU	455	B	3.5
189	5708	NZ	LYS	596	A	<-->	6721	CG	ASN	417	B	3.66
190	5708	NZ	LYS	596	A	<-->	6722	OD1	ASN	417	B	2.66
191	5708	NZ	LYS	596	A	<-->	6755	CB	TYR	421	B	3.45
192	5708	NZ	LYS	596	A	<-->	6756	CG	TYR	421	B	3.47
193	5708	NZ	LYS	596	A	<-->	6758	CD2	TYR	421	B	3.41
194	5708	NZ	LYS	596	A	<-->	7102	O	ARG	454	B	3.61
195	5708	NZ	LYS	596	A	<-->	7105	CA	LEU	455	B	3.73
196	5708	NZ	LYS	596	A	<-->	7110	C	LEU	455	B	3.48
197	5708	NZ	LYS	596	A	<-->	7111	O	LEU	455	B	2.72
198	5716	CA	ASP	597	A	<-->	7167	OD1	ASN	460	B	3.55
199	5722	O	ASP	597	A	<-->	7167	OD1	ASN	460	B	3.78
200	5718	CG	ASP	597	A	<-->	6709	CG2	THR	415	B	3.89
201	5718	CG	ASP	597	A	<-->	7168	ND2	ASN	460	B	3.67
202	5719	OD1	ASP	597	A	<-->	6709	CG2	THR	415	B	3.86
203	5719	OD1	ASP	597	A	<-->	7166	CG	ASN	460	B	3.65
204	5719	OD1	ASP	597	A	<-->	7168	ND2	ASN	460	B	2.66
205	5748	CA	LYS	600	A	<-->	7156	CA	SER	459	B	3.88
206	5758	O	LYS	600	A	<-->	7153	O	LYS	458	B	3.59
207	5758	O	LYS	600	A	<-->	7156	CA	SER	459	B	3.8
208	5758	O	LYS	600	A	<-->	7157	CB	SER	459	B	3.11

209	5749	CB	LYS	600	A	<-->	7156	CA	SER	459	B	3.67
210	5749	CB	LYS	600	A	<-->	7157	CB	SER	459	B	3.76
211	5749	CB	LYS	600	A	<-->	7162	N	ASN	460	B	3.56
212	5749	CB	LYS	600	A	<-->	7167	OD1	ASN	460	B	3.05
213	5750	CG	LYS	600	A	<-->	7167	OD1	ASN	460	B	3.6
214	5751	CD	LYS	600	A	<-->	7165	CB	ASN	460	B	3.77
215	5751	CD	LYS	600	A	<-->	7166	CG	ASN	460	B	3.37
216	5751	CD	LYS	600	A	<-->	7167	OD1	ASN	460	B	3.25
217	5751	CD	LYS	600	A	<-->	7168	ND2	ASN	460	B	3.9
218	5753	NZ	LYS	600	A	<-->	7168	ND2	ASN	460	B	3.65
219	5785	CE1	PHE	603	A	<-->	7331	O	GLY	476	B	3.64
220	5787	CZ	PHE	603	A	<-->	7327	N	GLY	476	B	3.88
221	5787	CZ	PHE	603	A	<-->	7329	CA	GLY	476	B	3.71
222	5787	CZ	PHE	603	A	<-->	7330	C	GLY	476	B	3.59
223	5787	CZ	PHE	603	A	<-->	7331	O	GLY	476	B	3.5
224	5796	C	VAL	604	A	<-->	7324	CB	ALA	475	B	3.86
225	5797	O	VAL	604	A	<-->	7323	CA	ALA	475	B	3.08
226	5797	O	VAL	604	A	<-->	7325	C	ALA	475	B	3.34
227	5797	O	VAL	604	A	<-->	7326	O	ALA	475	B	3.39
228	5797	O	VAL	604	A	<-->	7324	CB	ALA	475	B	3.34
229	5793	CB	VAL	604	A	<-->	7305	OH	TYR	473	B	3.35
230	5795	CG2	VAL	604	A	<-->	7305	OH	TYR	473	B	3.31
231	5800	CA	GLY	605	A	<-->	7325	C	ALA	475	B	3.74
232	5800	CA	GLY	605	A	<-->	7326	O	ALA	475	B	2.86
233	5800	CA	GLY	605	A	<-->	7324	CB	ALA	475	B	3.7
234	5801	C	GLY	605	A	<-->	7326	O	ALA	475	B	3.48
235	5803	N	TRP	606	A	<-->	7326	O	ALA	475	B	3.22
236	5803	N	TRP	606	A	<-->	7423	ND2	ASN	487	B	3.52
237	5818	O	TRP	606	A	<-->	7423	ND2	ASN	487	B	3.68
238	5823	OG	SER	607	A	<-->	7336	CG	ASN	477	B	3.38
239	5823	OG	SER	607	A	<-->	7337	OD1	ASN	477	B	3.8
240	5823	OG	SER	607	A	<-->	7338	ND2	ASN	477	B	3.15
241	5831	OG1	THR	608	A	<-->	7413	CE2	PHE	486	B	3.77
242	5831	OG1	THR	608	A	<-->	7414	CZ	PHE	486	B	3.29
243	5833	CG2	THR	608	A	<-->	7414	CZ	PHE	486	B	3.87
244	5840	CG	ASP	609	A	<-->	7338	ND2	ASN	477	B	3.76
245	5842	OD2	ASP	609	A	<-->	7336	CG	ASN	477	B	3.88
246	5842	OD2	ASP	609	A	<-->	7338	ND2	ASN	477	B	2.74

Table 9.9. *List of atom-atom interactions (Salt bridges) across protein-ligand interface in ACE2(chain A)-Spike Protein (Chain B) (BA.1variant) complex from PDBsum server*

Sl. No.	Atom no.	Atom name	Residue name	Residue no.	Chain Id	Salt bridges	Atom no.	Atom name	Residue name	Residue no.	Chain Id	Distance (Å)
1	2143	OE1	GLU	232	A	<-->	7486	NH1	ARG	493	B	2.67
2	5044	OE1	GLU	527	A	<-->	7589	ND1	HIS	504	B	3.76
3	5635	OE1	GLU	589	A	<-->	6598	NH2	ARG	403	B	3.89

Table 9.10. *List of atom-atom interactions (Hydrogen bonds) across protein-ligand interface in ACE2 (Chain A)-Spike Protein (Chain B) (BA.2 variant) complex from PDBsum server*

Sl. No.	Atom no.	Atom name	Residue name	Residue no.	Chain Id	Hydrogen bonds	Atom no.	Atom name	Residue name	Residue no.	Chain Id	Distance (Å)
1	258	NH1	ARG	357	A	<-->	5932	O	GLU	430	B	2.65
2	261	NH2	ARG	357	A	<-->	5917	OE1	GLN	429	B	3.11
3	261	NH2	ARG	357	A	<-->	5932	O	GLU	430	B	2.93
4	611	ND2	ASN	394	A	<-->	5917	OE1	GLN	429	B	2.92
5	922	OD1	ASP	427	A	<-->	7003	NZ	LYS	534	B	2.59
6	931	OD1	ASP	428	A	<-->	7003	NZ	LYS	534	B	2.59
7	947	N	THR	430	A	<-->	7029	OE2	GLU	536	B	2.68
8	1242	NZ	LYS	458	A	<-->	4045	OE2	GLU	232	B	2.57
9	1252	OG	SER	459	A	<-->	7440	ND2	ASN	580	B	3.1
10	1275	O	LEU	461	A	<-->	6979	NE2	GLN	531	B	2.87
11	1283	NZ	LYS	462	A	<-->	6946	OE1	GLU	527	B	2.58
12	1315	OE2	GLU	465	A	<-->	7462	NH1	ARG	582	B	2.8
13	1344	N	ILE	468	A	<-->	7539	OE2	GLU	589	B	3.02
14	1388	O	ILE	472	A	<-->	4003	NE2	HIS	228	B	2.79
15	1410	NE2	GLN	474	A	<-->	3965	OE2	GLU	224	B	2.64
16	1795	N	PHE	515	A	<-->	7028	OE1	GLU	536	B	3.32
17	1846	O	HIS	519	A	<-->	5829	NZ	LYS	419	B	2.76

Table 9.11. *List of atom-atom interactions (non-bonded contacts) across protein-ligand interface in ACE2 (Chain A)-Spike Protein (Chain B) (BA.2 variant) complex from PDBsum server.*

Sl. No.	Atom no.	Atom name	Residue name	Residue no.	Chain Id	Non-bonded contacts	Atom no.	Atom name	Residue name	Residue no.	Chain Id	Distance (Å)
1	228	NH1	ARG	355	A	<-->	7041	CD	PRO	538	B	3.63
2	257	CZ	ARG	357	A	<-->	5932	O	GLU	430	B	3.21

3	258	NH1	ARG	357	A	<-->	5931	C	GLU	430	B	3.72
4	258	NH1	ARG	357	A	<-->	5932	O	GLU	430	B	2.65
5	258	NH1	ARG	357	A	<-->	5935	CA	ASP	431	B	3.63
6	261	NH2	ARG	357	A	<-->	5915	CG	GLN	429	B	3.75
7	261	NH2	ARG	357	A	<-->	5916	CD	GLN	429	B	3.52
8	261	NH2	ARG	357	A	<-->	5917	OE1	GLN	429	B	3.11
9	261	NH2	ARG	357	A	<-->	5932	O	GLU	430	B	2.93
10	609	CG	ASN	394	A	<-->	5917	OE1	GLN	429	B	3.65
11	610	OD1	ASN	394	A	<-->	5916	CD	GLN	429	B	3.79
12	610	OD1	ASN	394	A	<-->	5917	OE1	GLN	429	B	3.54
13	610	OD1	ASN	394	A	<-->	5918	NE2	GLN	429	B	3.84
14	611	ND2	ASN	394	A	<-->	5916	CD	GLN	429	B	3.73
15	611	ND2	ASN	394	A	<-->	5917	OE1	GLN	429	B	2.92
16	913	CG	PRO	426	A	<-->	7026	CG	GLU	536	B	3.72
17	921	CG	ASP	427	A	<-->	7003	NZ	LYS	534	B	3.77
18	922	OD1	ASP	427	A	<-->	7002	CE	LYS	534	B	3.54
19	922	OD1	ASP	427	A	<-->	7003	NZ	LYS	534	B	2.59
20	930	CG	ASP	428	A	<-->	7001	CD	LYS	534	B	3.8
21	930	CG	ASP	428	A	<-->	7002	CE	LYS	534	B	3.86
22	930	CG	ASP	428	A	<-->	7003	NZ	LYS	534	B	3.42
23	931	OD1	ASP	428	A	<-->	7001	CD	LYS	534	B	3.73
24	931	OD1	ASP	428	A	<-->	7002	CE	LYS	534	B	3.46
25	931	OD1	ASP	428	A	<-->	7003	NZ	LYS	534	B	2.59
26	932	OD2	ASP	428	A	<-->	6999	CB	LYS	534	B	3.47
27	932	OD2	ASP	428	A	<-->	7001	CD	LYS	534	B	3.63
28	937	CA	PHE	429	A	<-->	7029	OE2	GLU	536	B	3.17
29	945	C	PHE	429	A	<-->	7029	OE2	GLU	536	B	3.4
30	938	CB	PHE	429	A	<-->	7029	OE2	GLU	536	B	3.81
31	939	CG	PHE	429	A	<-->	7029	OE2	GLU	536	B	3.7
32	940	CD1	PHE	429	A	<-->	7027	CD	GLU	536	B	3.59
33	940	CD1	PHE	429	A	<-->	7029	OE2	GLU	536	B	3.01
34	942	CE1	PHE	429	A	<-->	7029	OE2	GLU	536	B	3.76
35	947	N	THR	430	A	<-->	7029	OE2	GLU	536	B	2.68
36	949	CA	THR	430	A	<-->	7029	OE2	GLU	536	B	3.72
37	955	O	THR	430	A	<-->	7029	OE2	GLU	536	B	3.72
38	953	CG2	THR	430	A	<-->	7029	OE2	GLU	536	B	3.36
39	1222	CG	ARG	457	A	<-->	7458	CD	ARG	582	B	3.87
40	1224	NE	ARG	457	A	<-->	7458	CD	ARG	582	B	3.26
41	1226	CZ	ARG	457	A	<-->	7458	CD	ARG	582	B	3.26
42	1226	CZ	ARG	457	A	<-->	7459	NE	ARG	582	B	3.87
43	1230	NH2	ARG	457	A	<-->	7458	CD	ARG	582	B	3.27
44	1247	O	LYS	458	A	<-->	7398	CB	ALA	576	B	3.61
45	1238	CB	LYS	458	A	<-->	7438	CG	ASN	580	B	3.77
46	1238	CB	LYS	458	A	<-->	7440	ND2	ASN	580	B	3.52

47	1241	CE	LYS	458	A	<-->	4045	OE2	GLU	232	B	3.51
48	1241	CE	LYS	458	A	<-->	7438	CG	ASN	580	B	3.58
49	1241	CE	LYS	458	A	<-->	7439	OD1	ASN	580	B	3.15
50	1242	NZ	LYS	458	A	<-->	4043	CD	GLU	232	B	3.15
51	1242	NZ	LYS	458	A	<-->	4044	OE1	GLU	232	B	3.28
52	1242	NZ	LYS	458	A	<-->	4045	OE2	GLU	232	B	2.57
53	1242	NZ	LYS	458	A	<-->	7439	OD1	ASN	580	B	3.65
54	1251	CB	SER	459	A	<-->	7461	CZ	ARG	582	B	3.89
55	1251	CB	SER	459	A	<-->	7465	NH2	ARG	582	B	3.06
56	1252	OG	SER	459	A	<-->	7440	ND2	ASN	580	B	3.1
57	1252	OG	SER	459	A	<-->	7459	NE	ARG	582	B	3.68
58	1252	OG	SER	459	A	<-->	7461	CZ	ARG	582	B	3.66
59	1252	OG	SER	459	A	<-->	7465	NH2	ARG	582	B	2.78
60	1275	O	LEU	461	A	<-->	6979	NE2	GLN	531	B	2.87
61	1280	CG	LYS	462	A	<-->	6949	O	GLU	527	B	3.32
62	1280	CG	LYS	462	A	<-->	6975	CB	GLN	531	B	3.61
63	1281	CD	LYS	462	A	<-->	6949	O	GLU	527	B	3.68
64	1281	CD	LYS	462	A	<-->	6943	CB	GLU	527	B	3.86
65	1281	CD	LYS	462	A	<-->	6945	CD	GLU	527	B	3.88
66	1281	CD	LYS	462	A	<-->	6946	OE1	GLU	527	B	3.79
67	1282	CE	LYS	462	A	<-->	6949	O	GLU	527	B	3.89
68	1282	CE	LYS	462	A	<-->	6943	CB	GLU	527	B	3.38
69	1282	CE	LYS	462	A	<-->	6946	OE1	GLU	527	B	3.51
70	1283	NZ	LYS	462	A	<-->	6943	CB	GLU	527	B	3.43
71	1283	NZ	LYS	462	A	<-->	6945	CD	GLU	527	B	3.43
72	1283	NZ	LYS	462	A	<-->	6946	OE1	GLU	527	B	2.58
73	1283	NZ	LYS	462	A	<-->	7462	NH1	ARG	582	B	3.84
74	1295	O	PRO	463	A	<-->	7021	O	HIS	535	B	3.68
75	1295	O	PRO	463	A	<-->	7036	O	GLY	537	B	3.35
76	1291	CB	PRO	463	A	<-->	7021	O	HIS	535	B	3.37
77	1307	O	PHE	464	A	<-->	7036	O	GLY	537	B	3.82
78	1302	CD2	PHE	464	A	<-->	7030	C	GLU	536	B	3.72
79	1302	CD2	PHE	464	A	<-->	7032	N	GLY	537	B	3.14
80	1302	CD2	PHE	464	A	<-->	7034	CA	GLY	537	B	3.78
81	1304	CE2	PHE	464	A	<-->	7024	CA	GLU	536	B	3.78
82	1304	CE2	PHE	464	A	<-->	7025	CB	GLU	536	B	3.85
83	1304	CE2	PHE	464	A	<-->	7026	CG	GLU	536	B	3.34
84	1304	CE2	PHE	464	A	<-->	7027	CD	GLU	536	B	3.6
85	1304	CE2	PHE	464	A	<-->	7028	OE1	GLU	536	B	3.49
86	1304	CE2	PHE	464	A	<-->	7032	N	GLY	537	B	3.78
87	1305	CZ	PHE	464	A	<-->	7028	OE1	GLU	536	B	3.81
88	1312	CG	GLU	465	A	<-->	7499	CG	ASN	586	B	3.67
89	1312	CG	GLU	465	A	<-->	7500	OD1	ASN	586	B	3.16
90	1313	CD	GLU	465	A	<-->	7462	NH1	ARG	582	B	3.81

91	1315	OE2	GLU	465	A	<-->	7462	NH1	ARG	582	B	2.8
92	1315	OE2	GLU	465	A	<-->	7498	CB	ASN	586	B	3.77
93	1315	OE2	GLU	465	A	<-->	7499	CG	ASN	586	B	3.79
94	1333	C	ARG	466	A	<-->	7539	OE2	GLU	589	B	3.48
95	1334	O	ARG	466	A	<-->	7498	CB	ASN	586	B	3.4
96	1334	O	ARG	466	A	<-->	7539	OE2	GLU	589	B	3.8
97	1321	CB	ARG	466	A	<-->	7536	CG	GLU	589	B	3.68
98	1321	CB	ARG	466	A	<-->	7537	CD	GLU	589	B	3.47
99	1321	CB	ARG	466	A	<-->	7538	OE1	GLU	589	B	3.84
100	1321	CB	ARG	466	A	<-->	7539	OE2	GLU	589	B	3.58
101	1322	CG	ARG	466	A	<-->	7537	CD	GLU	589	B	3.66
102	1322	CG	ARG	466	A	<-->	7538	OE1	GLU	589	B	3.63
103	1322	CG	ARG	466	A	<-->	7539	OE2	GLU	589	B	3.72
104	1323	CD	ARG	466	A	<-->	7537	CD	GLU	589	B	3.52
105	1323	CD	ARG	466	A	<-->	7538	OE1	GLU	589	B	3
106	1327	NH1	ARG	466	A	<-->	7535	CB	GLU	589	B	3.27
107	1327	NH1	ARG	466	A	<-->	7538	OE1	GLU	589	B	3.41
108	1335	N	ASP	467	A	<-->	7539	OE2	GLU	589	B	3.25
109	1337	CA	ASP	467	A	<-->	7539	OE2	GLU	589	B	3.45
110	1342	C	ASP	467	A	<-->	7539	OE2	GLU	589	B	3.43
111	1339	CG	ASP	467	A	<-->	7457	CG	ARG	582	B	3.66
112	1339	CG	ASP	467	A	<-->	7458	CD	ARG	582	B	3.77
113	1340	OD1	ASP	467	A	<-->	7457	CG	ARG	582	B	3.47
114	1341	OD2	ASP	467	A	<-->	7457	CG	ARG	582	B	3.42
115	1341	OD2	ASP	467	A	<-->	7458	CD	ARG	582	B	3.05
116	1344	N	ILE	468	A	<-->	7539	OE2	GLU	589	B	3.02
117	1346	CA	ILE	468	A	<-->	7539	OE2	GLU	589	B	3.85
118	1347	CB	ILE	468	A	<-->	7539	OE2	GLU	589	B	3.6
119	1348	CG1	ILE	468	A	<-->	7489	CB	LEU	585	B	3.51
120	1348	CG1	ILE	468	A	<-->	7537	CD	GLU	589	B	3.88
121	1348	CG1	ILE	468	A	<-->	7539	OE2	GLU	589	B	3.23
122	1349	CG2	ILE	468	A	<-->	7537	CD	GLU	589	B	3.7
123	1349	CG2	ILE	468	A	<-->	7538	OE1	GLU	589	B	3.42
124	1349	CG2	ILE	468	A	<-->	7539	OE2	GLU	589	B	3.3
125	1350	CD1	ILE	468	A	<-->	7494	O	LEU	585	B	3.66
126	1350	CD1	ILE	468	A	<-->	7489	CB	LEU	585	B	3.81
127	1350	CD1	ILE	468	A	<-->	7562	CG	PHE	592	B	3.85
128	1350	CD1	ILE	468	A	<-->	7564	CD2	PHE	592	B	3.59
129	1353	N	SER	469	A	<-->	7491	CD1	LEU	585	B	3.85
130	1355	CA	SER	469	A	<-->	7491	CD1	LEU	585	B	3.57
131	1356	CB	SER	469	A	<-->	7491	CD1	LEU	585	B	3.78
132	1357	OG	SER	469	A	<-->	7491	CD1	LEU	585	B	3.78
133	1365	OG1	THR	470	A	<-->	4073	CG	PRO	235	B	3.54
134	1373	CB	GLU	471	A	<-->	4042	CG	GLU	232	B	3.33

135	1373	CB	GLU	471	A	<-->	4043	CD	GLU	232	B	3.75
136	1373	CB	GLU	471	A	<-->	4045	OE2	GLU	232	B	3.76
137	1387	C	ILE	472	A	<-->	4003	NE2	HIS	228	B	3.89
138	1388	O	ILE	472	A	<-->	4002	CE1	HIS	228	B	3.48
139	1388	O	ILE	472	A	<-->	4003	NE2	HIS	228	B	2.79
140	1406	CB	GLN	474	A	<-->	4003	NE2	HIS	228	B	3.87
141	1408	CD	GLN	474	A	<-->	3965	OE2	GLU	224	B	3.68
142	1409	OE1	GLN	474	A	<-->	4001	CD2	HIS	228	B	3.69
143	1410	NE2	GLN	474	A	<-->	3963	CD	GLU	224	B	3.49
144	1410	NE2	GLN	474	A	<-->	3965	OE2	GLU	224	B	2.64
145	1428	CA	ASN	477	A	<-->	3965	OE2	GLU	224	B	3.61
146	1435	C	ASN	477	A	<-->	3964	OE1	GLU	224	B	3.48
147	1435	C	ASN	477	A	<-->	3965	OE2	GLU	224	B	3.62
148	1436	O	ASN	477	A	<-->	3964	OE1	GLU	224	B	3.82
149	1437	N	LYS	478	A	<-->	3963	CD	GLU	224	B	3.44
150	1437	N	LYS	478	A	<-->	3964	OE1	GLU	224	B	3.17
151	1437	N	LYS	478	A	<-->	3965	OE2	GLU	224	B	3.3
152	1439	CA	LYS	478	A	<-->	3963	CD	GLU	224	B	3.78
153	1439	CA	LYS	478	A	<-->	3964	OE1	GLU	224	B	3.25
154	1448	C	LYS	478	A	<-->	3964	OE1	GLU	224	B	3.85
155	1450	N	PRO	479	A	<-->	3964	OE1	GLU	224	B	3.78
156	1454	CD	PRO	479	A	<-->	3962	CG	GLU	224	B	3.63
157	1454	CD	PRO	479	A	<-->	3963	CD	GLU	224	B	3.64
158	1454	CD	PRO	479	A	<-->	3964	OE1	GLU	224	B	3.2
159	1789	CA	SER	514	A	<-->	7028	OE1	GLU	536	B	3.9
160	1790	CB	SER	514	A	<-->	7028	OE1	GLU	536	B	3.57
161	1795	N	PHE	515	A	<-->	7028	OE1	GLU	536	B	3.32
162	1806	O	PHE	515	A	<-->	7028	OE1	GLU	536	B	3.56
163	1814	OE2	GLU	516	A	<-->	7072	NZ	LYS	541	B	3.81
164	1832	CD2	LEU	518	A	<-->	5793	CD	LYS	416	B	3.74
165	1845	C	HIS	519	A	<-->	5889	O	PRO	426	B	3.5
166	1846	O	HIS	519	A	<-->	5827	CD	LYS	419	B	3.17
167	1846	O	HIS	519	A	<-->	5828	CE	LYS	419	B	3.21
168	1846	O	HIS	519	A	<-->	5829	NZ	LYS	419	B	2.76
169	1846	O	HIS	519	A	<-->	5889	O	PRO	426	B	3.1
170	1838	CB	HIS	519	A	<-->	5825	CB	LYS	419	B	3.55
171	1838	CB	HIS	519	A	<-->	5827	CD	LYS	419	B	3.72
172	1839	CG	HIS	519	A	<-->	5825	CB	LYS	419	B	3.77
173	1840	ND1	HIS	519	A	<-->	5800	O	LYS	416	B	3.88
174	1841	CD2	HIS	519	A	<-->	5837	CA	SER	420	B	3.87
175	1842	CE1	HIS	519	A	<-->	5838	CB	SER	420	B	3.54
176	1842	CE1	HIS	519	A	<-->	5839	OG	SER	420	B	3.44
177	1843	NE2	HIS	519	A	<-->	5835	N	SER	420	B	3.81
178	1843	NE2	HIS	519	A	<-->	5837	CA	SER	420	B	3.43

179	1843	NE2	HIS	519	A	<-->	5838	CB	SER	420	B	3.35
180	1843	NE2	HIS	519	A	<-->	5839	OG	SER	420	B	3.76
181	1847	N	ALA	520	A	<-->	5889	O	PRO	426	B	3.49
182	1849	CA	ALA	520	A	<-->	5889	O	PRO	426	B	2.98
183	1851	C	ALA	520	A	<-->	5889	O	PRO	426	B	3.78
184	1853	N	PRO	521	A	<-->	5889	O	PRO	426	B	3.83
185	1856	CG	PRO	521	A	<-->	5892	CA	ASP	427	B	3.5
186	1857	CD	PRO	521	A	<-->	5889	O	PRO	426	B	3.27
187	1857	CD	PRO	521	A	<-->	5892	CA	ASP	427	B	3.52
188	1857	CD	PRO	521	A	<-->	5897	C	ASP	427	B	3.87
189	1857	CD	PRO	521	A	<-->	5898	O	ASP	427	B	3.83
190	1870	OG1	THR	523	A	<-->	5918	NE2	GLN	429	B	3.49

Table 9.12. *List of atom-atom interactions (Salt bridges) across protein-ligand interface in ACE2 (Chain A)-Spike Protein (Chain B) (BA.2 variant) complex from PDBsum server.*

Sl. No.	Atom no.	Atom name	Residue name	Residue no.	Chain Id	Salt bridges	Atom no.	Atom name	Residue name	Residue no.	Chain Id	Distance (Å)
1	923	OD2	ASP	427	A	<-->	7003	NZ	LYS	534	B	2.59
2	931	OD1	ASP	428	A	<-->	7003	NZ	LYS	534	B	2.59
3	1242	NZ	LYS	458	A	<-->	4045	OE2	GLU	232	B	2.57
4	1283	NZ	LYS	462	A	<-->	6947	OE2	GLU	527	B	2.58
5	1315	OE2	GLU	465	A	<-->	7462	NH1	ARG	582	B	2.8
6	1327	NH1	ARG	466	A	<-->	7539	OE2	GLU	589	B	3.41
7	1813	OE1	GLU	516	A	<-->	7072	NZ	LYS	541	B	3.81

9.4.1.5. Binding Free energy and per residue energy decomposition (PRED) analysis.

Binding free energies of the S protein (BA.1)-ACE2 and S protein (BA.2)-ACE2 complexes were calculated from the last 10 ns of the MD simulation once the system reached equilibrium using MM-GBSA approach. The values here represent only the relative binding free energy rather than absolute or total binding energy, as MM-GBSA approach uses a continuum solvent approach to determine the binding free energies of a system. The binding free energies determined for the BA.1 and BA.2 complexes along with the energy terms, were summarized in **Table 9.13**. From the **Table 9.13**, it can be seen that S protein (BA.2)-ACE2 (GB_{TOT}=-23.87 kcal/mol) complex was energetically more favourable than the S protein (BA.1)-ACE2 complex (GB_{TOT}=5.38 kcal/mol). Analysing **Table 9.13**, we observed that all the derived components for the BFE analysis contributed to the binding of S protein and ACE2 to form the S protein (BA.1 /BA.2)-ACE2 complex.

Table 9.13. *Binding free energies (kcal/mol) and its components of S protein (BA.1)-ACE2 and S protein (BA.2)-ACE2 complexes obtained using MM-GBSA approach.*

Energy components	$\Delta G_{(S\ protein(BA.1)-ACE2)} - [\Delta G_{S\ protein(BA.1)} + \Delta G_{ACE2}]$ (kcal/mol)		$\Delta G_{(S\ protein(BA.2)-ACE2)} - [\Delta G_{S\ protein(BA.2)} + \Delta G_{ACE2}]$ (kcal/mol)	
	Average	**std. dev. (±)**	**Average**	**std. dev. (±)**
VDW	-83.27	3.19	-133.43	6.45
ELE	-1176.79	22.22	-1595.14	34.34
GB	1275.85	21.42	1722.84	31.62
GBSUR	-10.39	0.2904	-18.13	0.43
GAS	-1260.06	21.45	-1728.57	33.18
GBSOL	1265.45	2134	1704.70	31.65
GBTOT	5.38	4.54	-23.87	6.38

To gain insights into the contribution of the individual amino acid residues to the overall PPI of the S protein (BA.1/BA.2)-ACE2 complexes, PRED values were calculated. In this analysis, the total binding energy was decomposed into residues to identify key residues for ACE2 binding to S protein (BA.1/BA.2). Essential residues with the binding energy value below -1.00 kcal/mol were shown in the **Figure 9.12 and 9.13**. The highest energy contributions for S protein (BA.1) come from the residues ARG408, TYR501, VAL503, TYR380, PHE377, THR376, ASP428, GLY502, PRO384, PRO499 while in S protein (BA.2) come from the residues LYS417, GLN498, GLN493, TYR505, PHE486, TYR449, TYR489, PHE456, ALA475, PHE490, LEU492 and LEU455.

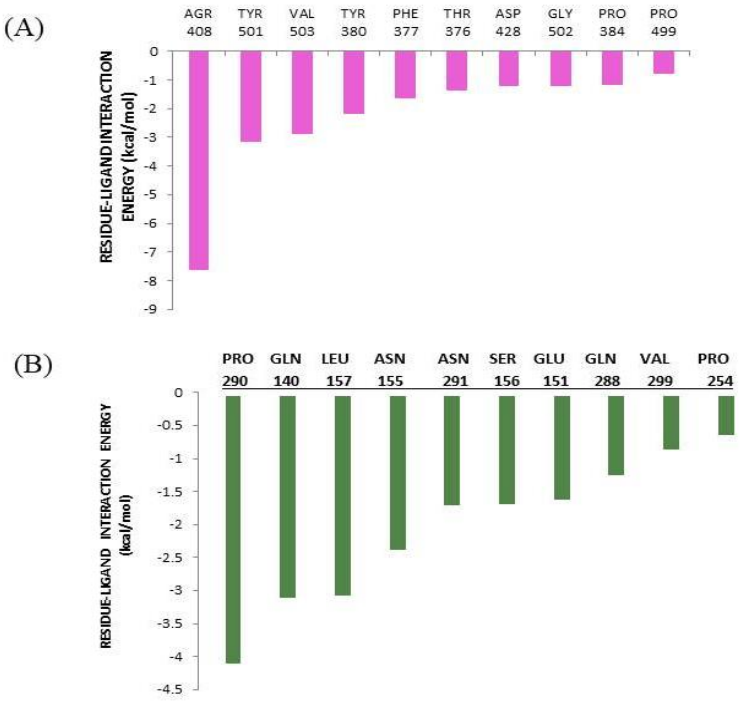

Figure 9.12. *Decomposition of binding free energy (kcal/mol) on per residue basis for* ***(A)*** *SPIKE (BA.1) and* ***(B)*** *ACE2 obtained using MM-GBSA approach.*

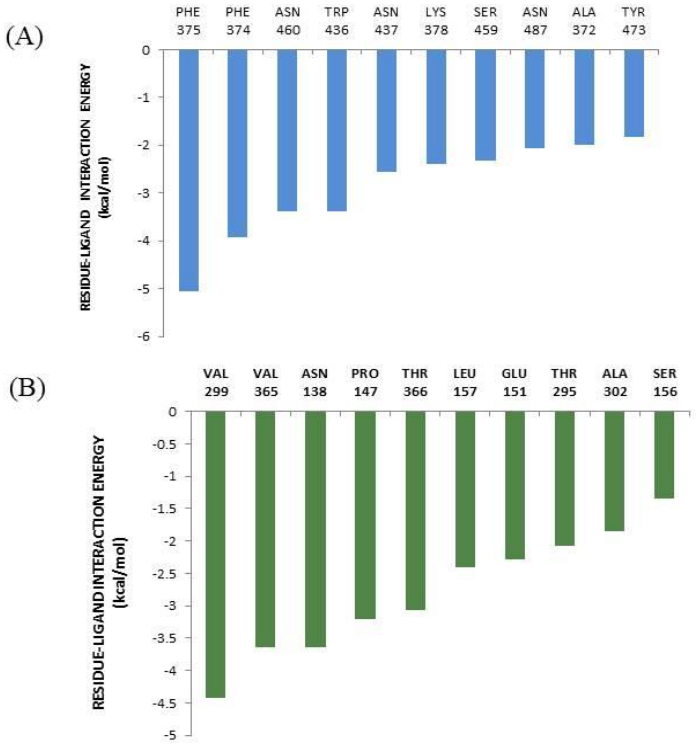

Figure 9.13. *Decomposition of binding free energy (kcal/mol) on per residue basis for* ***(A)*** *SPIKE (BA.2) and* ***(B)*** *ACE2 obtained using MM-GBSA approach.*

Discussion: The analysis performed in this study reveals that the SARS-CoV-2 BA.2 variant forms a more stable and stronger complex with the ACE2 receptor compared to BA.1 which was clearly visible from the lower RMSD and RMSF values for BA.2, particularly around the mutation sites indicating greater structural stability. Hydrogen bond and interface analyses further supported this, with BA.2 exhibiting more hydrogen bonds, a larger interface area, and more non-bonded contacts. Binding free energy calculations confirmed stronger binding in BA.2 than BA.1. Key residues such as GLN493, GLN498, and TYR505 that are mutated in both BA.1 and BA.2 contributed significantly to this enhanced binding, suggesting that these mutations may be the reason for increase in infectivity and transmissibility. Those key residues particularly around the mutation sites that contribute most significantly to the binding and stability of the spike-ACE2 complex, can act as "hotspot" regions for designing new ligands that can effectively disrupt this interaction.

9.5 Conclusions:

There is a lack of adequate data to say whether BA.1or BA.2 variant of SARS-CoV-2 virus is bringing a severer form of COVID-19 illness compared to the one witnessed during the first wave of the pandemic. It is unclear if the increased fatality is connected to either of the variant being deadlier or to the inflated volume of infections. The present study demonstrates the effect of this BA.1 and BA.2 omicron variant on SARS-CoV-2 RBD towards its binding with the ACE2 by employing MD simulation and other computational approaches. From the MD simulation of S protein (BA.1)-ACE2 and S protein(BA.2)-ACE2 complexes, we found the BA.2 causes extensive structural changes in the mutation region of spike protein in S protein(BA.2)-ACE2 complex. From the RMSD, RMSF, and number of inter-molecular hydrogen bond analysis, we found S protein (BA.2)-ACE2 complex to have enhanced stability than the S protein (BA.1)-ACE2 complex. The number of non-bonded contacts were also found to be higher in S protein(BA.2)-ACE2 complex. From the binding free energy calculations of the S protein(BA.1)-ACE2 and S protein(BA.2)-ACE2 complexes, we found that the affinity between S protein and ACE2 is higher in the BA.2 complex. The overall stability of the S protein(BA.2)-ACE2 complex and the increased affinity between S protein (BA.2) and ACE2 may result in higher virulence of the BA.2 strain than its BA.1 type strain. The salient interactions that we have reported across the S protein and ACE2 in the BA.1type and the BA.2 complexes could be used to design of novel inhibitors against the newly emerging coronavirus strains.

9.6. Bibliography:

[1]. Wu, Y. C., Chen, C. S., and Chan, Y. J. The outbreak of COVID-19: An overview. *Journal of the Chinese Medical Association,* 83(3): 217–220, 2020. https://doi.org/10.1097/JCMA.0000000000000270

[2]. Shereen, M. A., Khan, S., Kazmi, A., Bashir, N., and Siddique, R. COVID-19 infection: Origin, transmission, and characteristics of human coronaviruses. *Journal of Advanced Research,* 24: 91–98, 2020. https://doi.org/10.1016/j.jare.2020.03.005

[3]. Mizumoto, K., Kagaya, K., and Chowell, G. Effect of a wet market on coronavirus disease (COVID-19) transmission dynamics in China. *International Journal of Infectious Diseases,* 97: 96–101, 2020. https://doi.org/10.1016/j.ijid.2020.05.091

[4]. Kumar, S., Tao, Q., Weaver, S., Sanderford, M., Caraballo, M., Sharma, S., Pond, S., and Miura, S. An evolutionary portrait of the progenitor SARS-CoV-2 and its dominant offshoots in the COVID-19 pandemic. *Molecular Biology and Evolution,* 38(8):3046-3059, 2021. https://doi.org/10.1093/molbev/msab118

[5]. Woods, J. A., Hutchinson, N. T., Powers, S. K., Roberts, W. O., Gomez-Cabrera, M. C., Radak, Z., Berkes, I., Boros, A., Boldogh, I., Leeuwenburgh, C., Coelho-Júnior, H. J., Marzetti, E., Cheng, Y., Liu, J., Durstine, J. L., Sun, J., and Ji, L. L. The COVID-19 pandemic and physical activity. *Journal of Sports Science and Medicine,* 2(2): 55–64, 2022. https://doi.org/10.1016/j.smhs.2020.05.006

[6]. Lu, J., and Sun, P. D. High-affinity binding of SARS-CoV-2 spike protein enhances ACE2 carboxypeptidase activity. *Journal of Biological Chemistry,* 295(52): 18579–18588, 2020. https://doi.org/10.1074/jbc.RA120.015303

[7]. Thomas, S. The structure of the membrane protein of SARS-CoV-2 resembles the sugar transporter SemiSWEET. *Pathogens and Immunity,* 5(1): 342–363, 2020. https://doi.org/10.20411/pai.v5i1.377

[8]. Beniac, D. R., deVarennes, S. L., Andonov, A., He, R., and Booth, T. F. Conformational reorganization of the SARS coronavirus spike following receptor binding: Implications for membrane fusion. *PLOS ONE,* 2(10): e1082, 2007. https://doi.org/10.1371/journal.pone.0001082

[9]. Viana, R., Moyo, S., and Amoako, D. G., Tegally, H., Scheepers, C., Althaus, C..L, Anyaneji, U..J,, Bester, P.A., Boni, M.F., Chand, M., Choga, W.T., Colquhoun, R., Davids, M., Deforche, K., Doolabh, D., du Plessis, L., Engelbrecht, S., Everatt, J., Giandhari, J., Giovanetti, M., Hardie, D., Hill, V., Hsiao, N.Y.,

Iranzadeh, A., Ismail, A., Joseph, C., Joseph, R., Koopile, L., Kosakovsky Pond, S.L., Kraemer, M.U.G., Kuate-Lere, L., Laguda-Akingba, O., Lesetedi-Mafoko, O., Lessells, R.J., Lockman, S., Lucaci, A.G., Maharaj, A., Mahlangu, B., Maponga, T., Mahlakwane, K., Makatini, Z., Marais, G., Maruapula, D., Masupu, K., Matshaba, M., Mayaphi, S., Mbhele, N., Mbulawa, M.B., Mendes, A., Mlisana, K., Mnguni, A., Mohale, T., Moir, M., Moruisi, K., Mosepele, M., Motsatsi, G., Motswaledi, M.S., Mphoyakgosi, T., Msomi, N., Mwangi, P.N., Naidoo, Y., Ntuli, N., Nyaga, M., Olubayo, L., Pillay, S., Radibe, B., Ramphal, Y., Ramphal, U., San, J.E., Scott, L., Shapiro, R., Singh, L., Smith-Lawrence, P., Stevens, W., Strydom, A., Subramoney, K., Tebeila, N., Tshiabuila, D., Tsui, J., van Wyk, S., Weaver, S., Wibmer, C.K., Wilkinson, E., Wolter, N., Zarebski, A.E., Zuze, B., Goedhals, D., Preiser, W., Treurnicht, F., Venter, M., Williamson, C., Pybus, O.G., Bhiman, J., Glass, A., Martin, D.P., Rambaut, A., Gaseitsiwe, S., von Gottberg, A., and de Oliveira, T. Rapid epidemic expansion of the SARS-CoV-2 Omicron variant in southern Africa. *Nature,* 603(7902): 679-686*,* 2022. https://doi.org/10.21203/rs.3.rs-1516063/v1

[10]. Schmidt, F., Muecksch, F., and Weisblum, Y. Plasma neutralization of the SARS-CoV-2 Omicron variant. *New England Journal of Medicine,* 386(6):599-601, 2022. https://doi.org/10.1056/NEJMc2119641

[11]. Liu, L., Iketani, S., Guo, Y., Chan, J.F., Wang, M., Liu, L., Luo, Y., Chu, H., Huang, Y., Nair, M.S., Yu, J., Chik, K.K., Yuen, T.T., Yoon, C., To, K.K., Chen, H., Yin, M.T., Sobieszczyk, M.E., Huang, Y., Wang, H.H., Sheng, Z., Yuen, K.Y., and Ho, D.D. Striking antibody evasion manifested by the Omicron variant of SARS-CoV-2. *Nature,* 602(7898): 676-681, 2022. https://doi.org/10.1038/s41586-021-04388-0

[12]. Chen, L. L., Chu, A. W. H., Zhang, R. R. Q., Hung, I. F. N., and To, K. K. W. Serum neutralisation of the SARS-CoV-2 Omicron sublineage BA.2. *The Lancet Microbe,* 3(6): e404, 2022. https://doi.org/10.1016/S2666-5247(22)00060-X

[13]. Chen, L. L., Chua, G. T., and Lu, L. Omicron variant susceptibility to neutralizing antibodies induced in children by natural SARS-CoV-2 infection or COVID-19 vaccine. *Emerging Microbes and Infections,* 11(1):543-547*,* 2022. https://doi.org/10.1080/22221751.2022.2035195

[14]. Lu, L., Mok, B. W., Chen, L. L., Chan, J.M.C., Tsang, O.T.Y., Lam, B.H.S., Chuang, V.W.M., Chu, A.W.H., Chan, W.M., Ip, J.D., Chan, B.P.C., Zhang, R., Yip, C.C.Y., Cheng, V.C.C., Chan, K.H., Jin, D.Y., Hung, I.F.N., Yuen, K.Y., Chen, H., and To, K.K.W. Neutralization of SARS-CoV-2 Omicron variant by sera from BNT162b2 or CoronaVac vaccine recipients. *Clinical Infectious Diseases,* 75(1): e822-e826, 2021. https://doi.org/10.1093/cid/ciab1041

[15]. Chen, J., and Wei, G. W. Omicron BA.2 (B.1.1.529.2): High potential to becoming the next dominating variant. *Research Square,* rs.3.rs-1362445*, 2022*. https://doi.org/10.21203/rs.3.rs-1362445/v1

[16]. Chu, H., and Yuen, K. Y. Pathogenicity of SARS-CoV-2 Omicron. *EBioMedicine,* 12(5): e880, 2022. https://doi.org/10.1002/ctm2.880

[17]. Hoffmann, M., Krüger, N., Schulz, S., Cossmann, A., Rocha, C., Kempf, A., Nehlmeier, I., Graichen, L., Moldenhauer, A. S., Winkler, M. S., Lier, M., Dopfer-Jablonka, A., Jäck, H. M., Behrens, G. M. N., and Pöhlmann, S. The Omicron variant is highly resistant against antibody-mediated neutralization: Implications for control of the COVID-19 pandemic. *Cell*, 185(3): 447–456.e11, 2022. https://doi.org/10.1016/j.cell.2021.12.032

[18]. Gowrisankar, A., Priyanka, T. M. C., and Banerjee, S. Omicron: A mysterious variant of concern. *EPJ Plus,* 137: 100, 2022. https://doi.org/10.1140/epjp/s13360-021-02321-y

[19]. Rambaut, A., Holmes, E. C., Hill, V., McCrone, J. T., Ruis, C., du Plessis, L., and Pybus, O. G. A dynamic nomenclature proposal for SARS-CoV-2 lineages to assist genomic epidemiology. *Journal of Microbiology,* 5(11): 1403–1407, 2020. https://doi.org/10.1038/s41564-020-0770-5

[20]. Rahimi, F., and Bezmin Abadi, A. T. The Omicron subvariant BA.2: Birth of a new challenge during the COVID-19 pandemic. *International Journal of Surgery Case Reports,* 99: 106261, 2022. https://doi.org/10.1016/j.ijsu.2022.106261

[21]. Gupta, R. SARS-CoV-2 Omicron spike mediated immune escape and tropism shift. *Research Square,* 3: 1191837, 2022. https://doi.org/10.21203/rs.3.rs-1191837/v1

[22]. Berman, H. M., Westbrook, J., Feng, Z., Gilliland, G., Bhat, T. N., Weissig, H., Shindyalov, I. N., and Bourne, P. E. The protein data bank. *Nucleic Acids Research,* 28(1): 235–242, 2000. https://doi.org/10.1093/nar/28.1.235

[23]. Pettersen, E. F., Goddard, T. D., Huang, C. C., Couch, G. S., Greenblatt, D. M., Meng, E. C., and Ferrin, T. E. UCSF Chimera—A visualization system for exploratory research and analysis. *Journal of Computational Chemistry,* 25(13): 1605–1612, 2004. https://doi.org/10.1002/jcc.20084

[24]. Salomon-Ferrer, R., Gotz, A. W., Poole, D., Le Grand, S., and Walker, R. C. Routine microsecond molecular dynamics simulations with AMBER on GPUs. 2. Explicit solvent particle mesh Ewald. *Journal of Chemical Theory and Computation,* 9(9): 3878–3888, 2013. https://doi.org/10.1021/ct400314y

[25]. Jorgensen, W. L., Chandrasekhar, J., Madura, J. D., Impey, R. W., and Klein, M. L. Comparison of simple potential functions for simulating liquid water. *The Journal of Chemical Physics,* 79(2): 926–935, 1983. https://doi.org/10.1063/1.445869

[26]. Darden, T., York, D., and Pedersen, L. Particle mesh Ewald: An N·log(N) method for Ewald sums in large systems. *The Journal of Chemical Physics,* 98(12): 10089–10092, 1993. https://doi.org/10.1063/1.464397

[27]. Ryckaert, J.-P., Ciccotti, G., and Berendsen, H. J. C. Numerical integration of the Cartesian equations of motion of a system with constraints: Molecular dynamics of *n*-alkanes. *Journal of Computational Physics,* 23(3): 327–341, 1977. https://doi.org/10.1016/0021-9991(77)90098-5

[28]. Krautler V, Gunsteren W.F.V., and Hunenberger P.H. A fast SHAKE: Algorithm to solve distance constraint equations for small molecules in molecular dynamics simulations. *Journal of Computational Chemistry,* 22: 501-508, 2001. http://dx.doi.org/10.1002/1096-987X(20010415)22:53.0.CO;2-V

[29]. Berendsen, H. J., Postma, J. V., van Gunsteren, W. F., DiNola, A., and Haak, J. R. Molecular dynamics with coupling to an external bath. *The Journal of Chemical Physics,* 81(8): 3684–3690, 1984. https://doi.org/10.1063/1.448118

[30]. Laskowski, R. A., Hutchinson, E. G., Michie, A. D., Wallace, A. C., Jones, M. L., and Thornton, J. M. PDBsum: A web-based database of summaries and analyses of all PDB structures. *Trends in Biochemical Sciences,* 22(12): 488–490, 1997. https://doi.org/10.1016/s0968-0004(97)01140-7

[31]. Chen, F., Liu, H., Sun, H., Pan, P., Li, Y., Li, D., and Hou, T. Assessing the performance of the MM/PBSA and MM/GBSA methods. 6. Capability to predict protein–protein binding free energies and re-rank binding poses generated by protein–protein docking. *Physical Chemistry Chemical Physics,* 18(30): 22129–22139, 2016. https://doi.org/10.1261/rna.065896.118

[32]. Genheden, S., and Ryde, U. The MM/PBSA and MM/GBSA methods to estimate ligand-binding affinities. *Expert Opinion on Drug Discovery,* 10(5): 449–461, 2015. https://doi.org/10.1517/17460441.2015.1032936

[33]. Sun, H., Duan, L., Chen, F., Liu, H., Wang, Z., Pan, P., Zhu, F., Zhang, J. Z. H., and Hou, T. Assessing the performance of MM/PBSA and MM/GBSA methods. 7. Entropy effects on the performance of end-point binding free energy calculation approaches. *Physical Chemistry Chemical Physics*, 20(21): 14450-14460, 2018. https://doi.org/10.1039/C7CP07623A

[34]. Wang, E., Sun, H., Wang, J., Wang, Z., Liu, H., Zhang, J. Z. H., and Hou, T. End-point binding free energy calculation with MM/PBSA and MM/GBSA: Strategies and applications in drug design. *Chemical Reviews,* 119(16): 9478–9508, 2019. https://doi.org/10.1021/acs.chemrev.9b00055

[35]. Chen, J., Yin, B., Pang, L., Wang, W., Zhang, J. Z., and Zhu, T. Binding modes and conformational changes of FK506-binding protein 51 induced by inhibitor bindings: Insight into molecular mechanisms based on multiple simulation technologies. *Journal of Biomolecular Structure and Dynamics,* 38(7): 2141–2155, 2019. https://doi.org/10.1021/acs.jcim.0c01470

[36]. Du, Q., Qian, Y., Yao, X., and Xue, W. Elucidating the tight-binding mechanism of two oral anticoagulants to factor Xa by using induced-fit docking and molecular dynamics simulation. *Journal of Biomolecular Structure and Dynamics,* 38(2): 625–633, 2019. https://doi.org/10.1080/07391102.2019.1583605

[37]. Eduardo, S. C. E., Betancourt-Conde, I., Hernandez-Campos, A., Tellez-Valencia, A., and Castillo, R. In silico hit optimization toward AKT inhibition: Fragment-based approach, molecular docking, and molecular dynamics study. *Journal of Biomolecular Structure and Dynamics,* 37(16): 4301–4311, 2019. https://doi.org/10.1080/07391102.2018.1546618

[38]. Gao, J., Wang, Y., Chen, Q., and Yao, E. G. R. Integrating molecular dynamics simulation and molecular mechanics/generalized Born surface area calculation into pharmacophore modeling: A case study on the proviral integration site for Moloney murine leukemia virus (Pim)-1 kinase inhibitors. *Journal of Biomolecular Structure and Dynamics,* 38(2): 581–588, 2019. https://doi.org/10.1080/07391102.2019.1571946

[39]. Joshi, T., Joshi, T., Sharma, P., Chandra, S., and Pande, V. Molecular docking and molecular dynamics simulation approach to screen natural compounds for inhibition of Xanthomonas oryzae pv. Oryzae by targeting peptide deformylase. *Journal of Biomolecular Structure and Dynamics*, 39(3): 823-840, 2021. https://doi.org/10.1080/07391102.2020.1719200

[40]. Sk, M. F., Roy, R., and Kar, P. Exploring the potency of currently used drugs against HIV-1 protease of subtype D variant by using multiscale simulations. *Journal of Biomolecular Structure and Dynamics*, 39(3): 988-1003, 2021. https://doi.org/10.1080/07391102.2020.1724196

[41]. Tian, S., Ji, C., and Zhang, J. Z. H. Molecular basis of SMAC–XIAP binding and the effect of electrostatic polarization. *Journal of Biomolecular Structure and Dynamics*, 39(2): 743-752, 2021. https://doi.org/10.1080/07391102.2020.1713892

[42]. Wan, Y., Guan, S., Qian, M., Huang, H., Han, F., Wang, S., and Zhang, H. Structural basis of fullerene derivatives as novel potent inhibitors of protein acetylcholinesterase without catalytic active site interaction: insight into the inhibitory mechanism through molecular modeling studies. *Journal of Biomolecular Structure and Dynamics*, 38(2): 410-425, 2020. https://doi.org/10.1080/07391102.2019.1576543

[43]. Zhang, W., Yang, F., Ou, D., Lin, G., Huang, A., Liu, N., and Li, P. Prediction, docking study, and molecular simulation of 3D DNA aptamers to their targets of endocrine-disrupting chemicals. *Journal of Biomolecular Structure and Dynamics,* 37(16): 4274–4282, 2019. https://doi.org/10.1080/07391102.2018.1547222

[44]. Das, C., Hazarika, P. J., Deb, A., Joshi, P., Das, D., and Mattaparthi, V. S. K. Effect of Double Mutation (L452R and E484Q) in RBD of Spike Protein on its Interaction with ACE2 Receptor Protein. *Biointerface Research in Applied Chemistry*, 13(1): 97, 2023. https://doi.org/10.33263/BRIAC131.097